Sedimentary Geology
April 2021, Volume 415 Pages 105818 (25p.)
https://doi.org/10.1016/j.sedgeo.2020.105818
https://archimer.ifremer.fr/doc/00679/79082/

Upper Cretaceous to Palaeogene successions of the Gouaro anticline: Deepwater sedimentary records of the tectonic events that led to obduction in New Caledonia (SW Pacific)

Bordenave Aurélien [1, 2, 3, *] , Etienne Samuel [2], Collot Julien [2], Razin Philippe [3], Patriat Martin [4], Grélaud Carine [3], Agnini Claudia [5], Morgans Hugh [6], Guillemaut Flora [3], Moreau Armand [3]

[1] ADECAL Technopole, 1bis rue Berthelot, BP 2384, 98845 Nouméa, New Caledonia
[2] Geological Survey of New Caledonia (DIMENC), BP465, 98845 Nouméa Cedex, New Caledonia
[3] Université Bordeaux Montaigne/EA 4592 Géoressources & Environnement, 1 allée Fernand Daguin, 33607 Pessac Cedex, France
[4] IFREMER - Centre Bretagne - ZI de la Pointe du Diable, CS 10070, 29280 Plouzané, France
[5] Department of Geosciences, University of Padova, Padova, Italy
[6] GNS Science, Lower Hutt, New Zealand

* Corresponding author : Aurélien Bordenave, email address : aurelien.bordenave@ensegid.fr

Abstract :

In New Caledonia, upper Cretaceous to Palaeogene sedimentary rocks record a regional tectonic shift from Cretaceous extension to Eocene compression, which led to the obduction of oceanic mantle onto the northeastern tip of the submerged Zealandia continent. This study provides new descriptions of these successions in the region of the Gouaro anticline, from outcrops and an extensively cored, 1.9 km long onshore petroleum well, CADART-1. Combined sedimentological, palaeontological and mineralogical data allow us to propose a revised lithostratigraphic framework and to discuss sedimentary sources, basin physiography and vertical tectonic motions. The base of the studied section comprises an upper Cretaceous transgressive syn- to post-rift siliciclastic succession (Gouaro Formation) culminating in deepwater silicified mudstones. Our biostratigraphic analysis suggests that the Palaeocene and Lower Eocene are not present in the studied section. During the middle Eocene, sedimentation is dominated by deepwater pelagic carbonates and calciturbidites (Adio Limestone). The middle to upper Eocene is marked by a 4 km thick, lithologically heterogeneous turbidite succession, the Bourail Flysch Group, divided into: (i) the Lutetian to Bartonian Lower Bourail Flysch Formation, comprising mixed siliciclastic - calcareous turbidites; (ii) the Bartonian to Priabonian Middle Bourail Flysch Formation, dominated by calcareous turbidites; and (iii) the uppermost Eocene (to Oligocene?) Upper Bourail Flysch Formation consisting of clinopyroxene-rich volcaniclastic turbidites and extraformational breccias. Two successive phases of clastic fluxes occurred, the former during the Lutetian-Bartonian and the latter during the uppermost Priabonian, separated by a period of drowning and/or subsidence during the Bartonian to Priabonian. These phases are likely controlled by vertical motions and we discuss their possible tectonic origin. Of particular note is that we believe that within the Bourail Basin, horizontal shortening and nappe emplacement are only recorded during the latest Eocene and possibly Oligocene. Indeed, the second phase of clastic flux is associated with debris flow breccia, possibly derived from a thrust front, yet we discuss alternative origins such as fault scarp erosion or intraslope failures.

Keywords : Zealandia, New Caledonia, Upper Cretaceous, Palaeogene, Turbidite, Obduction

1. Introduction

Obductions are unusual tectonic events observed in a number of locations worldwide (e.g., Oman, Cuba, Taiwan). Generally, both the ophiolite and the associated sedimentary basins are poorly preserved and/or strongly tectonised due to imbrication within the orogenic belts (Lagabrielle and Cannat, 1990; Kerr et al., 1998; Manatschal and Müntener, 2009). In New Caledonia, one of the largest ophiolitic peridotites of the world covers one third of the main island, Grande Terre (Fig. 1). This weakly deformed nappe is thought to have been emplaced in the latest Eocene on the continental Norfolk Ridge (Cluzel et al., 2001; Maurizot et al., 2020b). The tectonic mechanisms by which such mantle ophiolites are emplaced remain enigmatic in the theory of plate tectonics. Two main competing sets of models are proposed. In the first one, obduction is the result of a continental subduction zone or arc-continent collision that leads to the emplacement of a supra-subduction forearc mantle and crust (e.g., Dewey et al.1976; Aitchison et al., 1998; Gautier et al., 2016). In the second one, obduction occurs as a back-thrust of the main subduction thrust, often in the context of a ridge-trench interaction (e.g., Dewey et al., 1976; Tokuyama et al., 1992; Mortimer et al., 2003; Boudier and Nicolas, 2020). Other recent models invoke mechanisms implying vertical motions rather that horizontal shortening (Lagabrielle et al., 2013; Sutherland et al., 2020). In New Caledonia, a thick sedimentary succession underlying the ophiolite, spanning the upper Cretaceous to the uppermost Eocene, is preserved and records a succession of tectonic events that is thought to ultimately lead to obduction. These unique records are not only of regional significance, with the large scale geodynamic changes affecting New Caledonia and the Zealandia continent, but are also of global interest for understanding tectonic processes that can generate obduction. On the western coast of Grande Terre, more specifically within the Gouaro anticline in the Bourail area (Fig. 1), a 4 km thick sedimentary succession is particularly well-preserved. The basal ~1.9 km of the section (Senonian to lower Priabonian) has been cored by the CADART-1 onshore exploration well, whereas the remaining ~1.8 km upper section (lower Priabonian to supposed latest Priabonian) crops out along natural exposures. In this paper, we present a detailed characterisation of this section with high resolution sedimentological descriptions coupled with mineralogical, hyperspectral and biostratigraphic analyses. We propose a new lithostratigraphic framework and provide alternatives for the evolution of sediment sources. This allows us to reconstruct the vertical motions that affected Norfolk Ridge during the Palaeogene and hence discuss the origin of the tectonic events that affected the ridge just before obduction. Resolving these issues is critical for understanding obduction mechanisms in the broader context of northern Zealandia tectonics.

2. Geological setting

2.1 Overview of the geology of New Caledonia in its regional tectonic context

New Caledonia is located on the continental Norfolk Ridge at the northeastern extremity of the submerged Zealandia continent (Mortimer et al., 2017) (Fig. 1a). From the late Carboniferous to the early Cretaceous, the Norfolk Ridge is thought to have been located in the fore-arc domain of a subduction zone where the Phoenix plate dipped towards the southwest beneath the eastern active margin of the Gondwana supercontinent (Mortimer et al., 2009; Cluzel et al., 2010). In New Caledonia, this active margin phase resulted in the collage of (i) arc-derived sediments (Meffre, 1991; Aitchison and Meffre, 1992), (ii) an accretionary complex, and (iii) slices of oceanic crust and mantle (Meffre et al., 1996; Cluzel and Meffre, 2002). For clarity, these terranes are regrouped in this paper as the "Sedimentary Basement" (e.g., Figs.1b, 2). Following this active margin stage, a phase of Cretaceous rifting (ca. 110-100 Ma to ca. 85 Ma) led to the dislocation of the eastern Gondwana margin and initiated the separation of Zealandia from Gondwana (Gaina et al., 1998; Crawford et al., 2003; Sdrolias et al., 2003; Schellart et al., 2006; Whattam et al., 2008; Collot et al., 2020). This rifting stage is followed by seafloor spreading in the Tasman Sea, during the late Cretaceous to the late Palaeocene, inducing regional post-rift tectonic inactivity and generalised thermal subsidence (Hayes and Ringis, 1973; Weissel and Hayes, 1977; Gaina et al., 1998). Subsequently, in the Eocene, a major change in the tectonic regime from extension to compression occurred

(Aitchison et al., 1995; Sutherland et al., 2017; Collot et al., 2020). This Eocene convergence phase profoundly affected the geology of Zealandia (Aitchison et al., 1995; Maurizot and Cluzel, 2014; Sutherland et al., 2017) and in New Caledonia culminated with the westward emplacement of oceanic mantle onto the continental crust of the Norfolk Ridge (Aitchison et al., 1995; Cluzel et al., 2001; Maurizot and Cluzel, 2014). This obduction is thought to result from the locking of a NE-dipping subduction zone due to the arrival of the Norfolk Ridge in the subduction trench (Paris, 1981; Aitchison et al., 1995; Cluzel et al., 2006). This convergence generated a high pressure - low temperature (HP-LT) metamorphic core complex exhumed during the late Eocene (Baldwin et al., 2007; Vitale Brovarone et al., 2018), which now crops out in the northeastern part of Grande Terre (Fig. 1b). During the Eocene, this collisional episode led to the stacking of several allochthonous nappes over the Norfolk Ridge (Figs. 1b, 2): (i) the Montagnes Blanches Nappe (Maurizot, 2011), composed of upper Cretaceous-Palaeogene sedimentary deposits; (ii) the Poya Nappe (Cluzel et al., 1997, 2001, 2018) comprising oceanic basalts and abyssal argillites, interpreted to be the oceanic crust of the subducting plate, as well as Coniacian to Campanian turbidite sandstones (Paris, 1981; Cluzel et al., 2018; Maurizot et al., 2020a); and (iii) the Peridotite Nappe (Avias, 1967), which is interpreted to be the supra-subduction zone fore-arc lithosphere (Cluzel et al., 2006, 2020; Secchiari et al., 2017). These three nappes overlie the parautochthonous sedimentary units of the Norfolk Ridge (Fig. 2). These sedimentary units spanning the upper Cretaceous to the Palaeogene rest unconformably on the Sedimentary Basement and are thought to record both the regional rifting phase and the Eocene convergence phase. These units, typically referred to as the “Sedimentary Cover”, are presented in detail in Section 2.2. The Peridotite Nappe was emplaced sometime between 34 and 27 Ma. Indeed, the youngest sediments underling the ophiolite are dated by biostratigraphy as being ca. 34 Ma (Cluzel, 1998; Cluzel et al., 2001, Maurizot et al., 2020a) and the Koum and St Louis granitoids that seal the ophiolite are dated at 27 Ma (Cluzel et al., 2005; Paquette and Cluzel, 2006). Following this compressional event, which led to the onset of the ophiolitic complex, most of the region entered a phase of back-arc basin opening related to the eastward retreat of the Tonga-Kermadec subduction zone (Auzende et al., 1988; Pelletier et al., 1998; Mortimer et al., 2007). Post-obduction isostatic re-equilibrium of the Norfolk Ridge led to the exhumation of all tectonic units (Lagabrielle et al., 2005; Chardon and Chevillotte, 2006) and emplacement of shallow water carbonate platforms, the Nepoui Limestone (Maurizot et al., 2016; Tournadour et al., 2020).

2.2 Upper Cretaceous to Palaeogene stratigraphic units of New Caledonia

Figure 2 provides a lithostratigraphic summary of the main units of the upper Cretaceous to Palaeogene Sedimentary Cover of New Caledonia, which lies on the Sedimentary Basement and is overlain by the nappes. The regional syn-rift phase, spanning from the Cenomanian to Mid-Campanian, is recorded by fluvial conglomerates and shallow marine coal-bearing sandstones forming the "Formation à Charbon" (Paris, 1981) along with rift-related volcanism (Pic Jacob volcanic Formation (Tissot and Noesmoen, 1958; Cluzel et al., 2011; Maurizot et al., 2020a). The post-rift phase is recorded by Mid-Campanian to Palaeocene transgressive succession comprising calcareous siltstones ("Mamelons Rouges Beds Formation") followed by silicified deepwater mudstones ("Black Chert Formation"). From the Palaeocene to the middle Eocene (Maurizot, 2011), a shift to fully marine, carbonate-dominated sedimentation is recorded by the deposition of ca. 150 m thick pelagic calcareous mudstones, mostly exposed on the Montagnes Blanches Nappe in the Koumac region ("*Globigerina* Limestones") (Figs. 1b, 2) as well as by calciturbidites and carbonate debris flow breccia (e.g., "Adio Limestones", "Creek Aymes Limestones", "Buadio Breccia") (Gonord, 1977;

Paris, 1981; Maurizot, 2011, 2012). These carbonate deposits have previously been restricted to the Palaeocene and lower Eocene (Maurizot and Cluzel, 2014), but recent stratigraphic studies (Dallanave et al., 2018, 2020) and new biostratigraphic analyses documented in this study suggest that they only span from the lower to middle Eocene (Section 3.3). Previous studies attributed the development of these carbonates to (i) a continuation of post-rift thermal subsidence (Paris, 1981), (ii) a regional plate motion change associated with the initiation of the Tonga-Kermadec subduction (Dallanave et al., 2018, 2020), (iii) global palaeoclimatic changes (Hancock et al., 2003; Hollis et al., 2005; Hollis, 2007) or (iv) local pre-obduction tectonics (Maurizot, 2012, 2014; Maurizot and Cluzel, 2014). Following this succession, the middle to upper Eocene onset of convergence is thought to have resulted in the deposition of mixed source turbidites known as the “Eocene Flysch” (Gonord, 1977), the “Bourail Flysch” (Paris, 1981), or the “Palaeogene Flysch” (Cluzel et al., 1998). The latter typically overlies pelagic carbonate formations and mostly crops out along the western coast of Grande Terre. The succession has been recently documented as the “Bourail Flysch Group” (Fig. 2) (Maurizot, 2011; Maurizot and Cluzel, 2014; Maurizot et al., 2020a) with three distinct formations: (i) the “Lower Bourail Flysch”, described as middle to late Eocene calciturbidites, (ii) the “Upper Bourail Flysch”, described as late Eocene volcaniclastic turbidites and (iii) the latest Eocene “Olistostrome”, dominated by polygenic breccia and outsized blocks (Maurizot and Cluzel, 2014; Maurizot et al., 2020a). Contemporaneous shallow water carbonate platforms are known to have developed throughout the Eocene in the region. This is clearly observed in the Uitoé area where the upper Eocene "Uitoé Limestones” lie unconformably on the Triassic sedimentary basement (Tissot and Noesmoen, 1958; Gonord, 1977; Paris, 1981; Maurizot, 2014). In addition, the reworking of shallow water carbonate components is common within all the Eocene flyschs (Routhier, 1953; Paris, 1981; Maurizot and Cluzel, 2014; Maurizot et al., 2020a). To explain such a succession, a depositional model involving a foreland basin has been proposed (Maurizot, 2014; Maurizot and Cluzel, 2014; Maurizot et al., 2020a). This flexural basin would have formed in front of subduction/obduction-related thrust nappes, ie. the Montagnes Blanches Nappe, the Poya Nappe and the Peridotite Nappe. The overall coarsening and thickening upward trend of the Bourail Flysch Group is interpreted as reflecting the propagation of thrust nappes prior to obduction (Maurizot and Cluzel, 2014; Maurizot et al., 2020a). Calciturbidites of the Lower Bourail Flysch would be derived from shallow water carbonate platforms developed on a peripheral forebulge (Maurizot, 2014; Maurizot et al., 2020a), whereas volcaniclastic turbidites of the Upper Bourail Flysch would originate from the erosion of basalts of the Poya Nappe. In turn, breccia and olistoliths of the "Olistrostrome" originate from the gravitational destabilisation of sedimentary units of the Montagnes Blanches Nappe, more specifically the "Black Chert" and "*Globigerina* Limestones" formations (Maurizot, 2011; Maurizot and Cluzel, 2014; Maurizot et al., 2020a).

2.3 Study area: the Gouaro anticline

The Gouaro anticline is located on the western coast of Grande Terre, in the Bourail region (Figs. 1b, 3). It is part of a folded structure comprising sedimentary cover, allochthonous nappes and possibly the Sedimentary Basement (Fig. 3) (Maurizot and Cluzel, 2014). This 30 km-long, 10 km wide and 135°N oriented anticline plunges towards the northwest to form a pericline in the Cap Goulvain area (Fig. 3a). In the north and northeast part of the study area, the anticline incorporates the Montagnes Blanches Nappe and the Poya Nappe (Fig. 3b). To the southeast, it displays a successive Palaeogene to upper Cretaceous sedimentary cover and Mesozoic sedimentary basement outcrops. The anticline axis was a target for petroleum exploration with several hydrocarbon exploration boreholes: Gouaro 1 and 2, completed in the 1950's (Pomeyrol, 1955), and CADART-1 in 1999 (France, 2000) (Fig. 3b). Located on the left bank of the Nera River, close to its mouth (Fig. 3a), CADART-1 was drilled to 1930 m depth. A total of 1777 m of core was recovered between -153 m and the bottom of the hole. Our study focuses on the 4 km thick composite succession of upper Cretaceous to Palaeogene deposits recorded in the CADART-1 well and at outcrops along the Nera River section (Fig. 3a). The lower half of the sedimentary section is dated as upper Cretaceous to late Eocene while the upper part is yet to be stratigraphically constrained but is hypothesised to date from the latest Eocene (Maurizot and Cluzel, 2014; Maurizot et al., 2020a).

3. Methods

3.1 Sedimentology

Detailed sedimentological observations were performed both in the field and on the CADART-1 cores. They were reported on conventional sedimentological logs at 1:50 scale, subsequently synthesised at 1:500 and 1:5000 scales. A facies analysis was undertaken, with particular attention given to sedimentary structures, grain size trends, laminations, bedding, bed contacts, trace fossils, mineralogical and palaeontological content (Fig. 4). Beds less than 5 cm thick were not drawn on the 1:50 scale logs. The terminology proposed by Stow (2005) for bedding and lamination scales was used. Such observations allowed the elaboration of a comprehensive, process-based facies classification, which uses classical turbidite facies models developed by Bouma (1962) and Mutti (1992). Sedimentary facies were regrouped into 10 facies associations and subdivided into two main groups depending on their composition, either as mixed calcareous, siliciclastic, clinopyroxene-rich (cpx-rich) facies associations (FAm; see Table 1), or as calcareous-dominated facies associations (FAc; see Table 1). For the latter, the Dunham (1962) classification was used to describe rock textures. These facies associations form the basis of our sedimentary process and depositional environment interpretations.

3.2 Biostratigraphy

Biostratigraphic data from benthic and planktonic foraminifera used in this study are a combination of analyses from the ERADATA company, partly published by Maurizot and Cluzel (2014) and new analyses performed by GNS Science. Identifications rely on the foraminiferal taxa illustrated by Jenkins (1971), Hornibrook et al. (1989), Olsson et al. (1999), Berggren and Pearson (2005), Pearson et al. (2006). Taxa identifications were mostly performed on thin sections, therefore the ages given in this study are limited to stages and not biozones (e.g., Bartonian rather than E12 / E13). Analyses of calcareous nannofossil assemblages were also performed on 50 samples spanning the interval from -1614 m to the top of the section. Smear slides were prepared from raw material following standard procedures described in Bown and Young (1998). Areal semi-quantitative counts on three long transects (ca. 6-7 mm^2) have been carried out using a Zeiss transmitted light microscope at x1250 magnification. The taxonomy adopted is that of Aubry (1984, 1988, 1989, 1990, 1999), Perch Nielsen (1985), Bown (2005), and Agnini et al. (2014). Calcareous nannofossil biostratigraphy is used to date the section, applying the biozonation schemes of Martini (1971) and Agnini et al. (2014). Calcareous nannofossil events reported in Agnini et al. (2014) have been recalibrated to the Geological Time Scale GTS2012 (Gradstein et al., 2012).

3.3 Petrographic analyses

Petrographic observations were performed on a microscope with plane and cross-polarised light (PPL/XPL) on more than 110 thin sections from samples distributed along the section. These qualitative observations were supplemented by quantitative point count analyses made on the Eocene Bourail Flysch Group. Fifteen representative thin sections of the latter were selected on samples of similar grain-size (medium-grained sands) (see Fig. 4 for sample locations). On each thin section, the relative proportion of the rock components were quantified on the same surface area (6 cm^2). A random grid point counting method (Flügel, 2013) was performed with the JMicroVision Image analysis software. This stochastic method consists of a count of 688 elements randomly chosen by the software on 16 different images of the thin section. Quantified mineralogical and palaeontological components were regrouped into nine main classes: quartz, feldspar, silicified mudrock, calcareous clast, siliciclastic clast, metamorphic clast, clinopyroxene, benthic foraminifera and planktonic foraminifera (see Appendix A). These classes are thought to reflect the overall variations and importance of the mineralogical fraction. Element abundances were categorised as trace (<1%); rare (1%–10%); common (>10%–25%); abundant (>25%–50%); dominant (>50%).

3.4 Hyperspectral analysis

High-resolution imaging and reflectance spectroscopy analysis of the CADART-1 cores were undertaken by CSIRO with their HyLogger^{TM}-3 core scanner (Fig. 4). Reflectance spectroscopy studies the interaction between light and matter such as minerals or rocks (Clark et al., 1990). In the case of the HyLogger^{TM}-3 core scanner, reflected wavelength allows us to identify the main mineralogical components of scanned rocks and determine the presence, relative abundance and composition of the mineral phase. This method allows continuous measurements to be performed along all cores. The reflectance spectra were resampled to 8 nm spectral resolution and 1 cm spatial resolution with "The Spectral Geologist" software (TSG^{TM}). Three best matched minerals mix were extracted along with estimates of their relative proportions for each wavelength range (e.g., VNIR, SWIR and TIR) and fitting errors. Differences between the VNIR / SWIR and TIR summary distribution plots arise from the different spectrally active bands or absorption features that a phase exhibits. In this study, scanner results were only used on mineralogical group identifications on both wavelength domains (silicates instead of quartz, sulphate instead of gypsum or pyrite) because mineral identification can be biased by core conditions (e.g., humidity, core roughness). The relative abundance of mineralogical components analysed by hyperspectral techniques will be noted in this study, however the results from the point counting technique is favoured for its robustness. To calibrate Hylogging spectral dataset, 30 samples were selected for bulk, random powder XRD analysis to provide a validated mineralogical framework of the mineralogy identified spectrally. Details on the instrumentation, operational set-up and general processing procedures can be found in Mason and Huntington (2012).

4. Results

Figure 4 summarises our newly acquired data along the CADART-1 / Nera River section with stratigraphy, lithostratigraphic units, hyperspectral data, a composite log showing the evolution of lithology and sedimentary facies and the position of samples. The base of the section, which corresponds to the lowermost cored interval of CADART-1, comprises a first unit of alternating muddy sandstones and siltstones, newly named the “Gouaro Formation”. It is overlain by an uppermost Cretaceous hemipelagic siltstone unit defined previously by Maurizot and Cluzel (2014) as the “Mamelons Rouges Beds Formation”. These two siliciclastic formations are sharply overlain by a middle Eocene calcareous unit that we link with the “Adio Limestone Formation” (Maurizot, 2012; Maurizot et al., 2020a). The stratigraphic gap between the uppermost Cretaceous and the middle Eocene, is attributed here to a tectonic contact (see Section 4.4). Overlying the Adio Limestone Formation is the 3.5 km thick turbidite succession of the Bourail Flysch Group that, based on the following analyses, has been subdivided into the Lower, Middle and Upper Bourail formations. In the following sections, we provide a detailed description of sedimentary facies and internal organisation, mineralogical composition, palaeontological data and main sedimentary unit boundaries of all lithostratigraphic formations identified in the CADART-1 /Nera River section.

4.1 Sedimentology and stacking pattern of units

The Gouaro Formation is a 210 m thick unit, between the bottom of the hole at -1930 m and -1720 m (Fig. 4), composed of five main facies associations (Fig. 5a). These facies associations correspond to FAm1, FAm2, FAm3, FAm4 and FAm5. The latter are described in Table 1. Noteworthily, some dewatering structures such as pillars, convolute, dishes or flame structures due to the upward flow of water loosening the packing of sediment grains are rarely present in FAm2. FAm5 differs from FAm4 due to its finer grain size and the lack of a basal massive sandstone interval. Highly deformed, decimetre-thick organic matter-rich layers are observed within all facies associations (FAm1-FAm5). As shown on the detailed logs in Figure 6, the unit is organised following roughly symmetrical, coarsening to fining upward and thickening to thinning upward, decametre-thick sand-dominated packages composed of facies associations FAm2 and FAm3 separated by mud-dominated intervals composed of facies associations FAm6 and FAm4/5 (Fig. 6b).

Conformably overlying the Gouaro Formation, the “Mamelons Rouges Beds Formation” spans -1720 m and -1616 m depth in the CADART-1 well (Fig. 4). It mostly consists of heavily bioturbated (*Planolites, Phycosiphon*) siltstones regrouped within facies association FAm6 (Fig. 6). FAm5 is rarely observed. In some places, several decimetre to metre-thick, highly fractured organic matter-rich layers are present.

At -1615 m depth, the Adio Limestone Formation marks a significant lithological change from the underlying deposits. This 79 m thick interval (-1615 m to -1536 m) comprise four main facies associations (Fig. 7): (1) thick-bedded, sharp to erosively based, normally graded, coarse to medium-grained, structureless to planar-laminated bioclastic grainstones (FAc1); (2)

faintly planar-laminated and/or soft-sediment deformed bioclastic packstones (FAc2); (3) bioturbated, massive to locally soft-sediment deformed bioclastic wackestones (FAc3); (4) massive calcareous mudstones with siliceous nodules, calcite veins and abundant horizontal to vertical stylolites (FAc4). The formation is organised following a coarsening upward bioclastic interval with successive facies associations FAc3, FAc2, FAc1. The top of the formation is composed of the FAc4 micritic mudstones with a sharp basal contact with FAc1 (Fig. 8).

The Adio Limestone Formation is overlain by the siliciclastic Lower Bourail Flysch Formation. This 801 m thick unit, located between -1536 m and -735 m depth in the well, is composed of bioturbated siltstones, interbedded very fine-grained sandstones and siltstones, as well as amalgamated coarse-grained sandstones of facies associations FAm6, FAm5, FAm4, FAm3 and FAm2 (Fig. 9). FAm3 and FAm2 are well represented. The Lower Bourail Flysch is divided into a lower part dominated by FAm6 and an upper part organised following two ca. 100-150m thick sandy packages (Figs. 4, 10b). These sandy packages are organised into symmetrical, thickening and coarsening upward (FAm5 to FAm2) to thinning and fining upward successions (FAm2 to FAm5) (Fig. 10b). FAm2 is more prominent in the first interval (53 m thick) than the second (33 m thick). These two sandy packages are separated by a ca. 240 m thick silty interval comprising unorganised facies associations FAm6 and FAm5.

The Middle Bourail Flysch Formation has been described at the top of the well and along the first half of the Nera River section (Fig. 4). This 1.5 km thick interval is primarily composed of thinly bedded calcareous sandstones alternating with bioturbated siltstones and mudstones (Fig. 11a). Facies associations FAm6, FAm5 and FAm4 are dominant. Bed bases are generally sharp and bed tops are typically ripple-laminated (Fig. 11b). The formation is organised into asymmetrical metre-thick, coarsening and thickening upward successions involving facies associations FAm5 and FAm4 (Fig. 11a). Outcrops along the Nera River section reveal beds that are laterally isopaceous and continuous.

The top of this section is composed of the Upper Bourail Flysch Formation. Cropping out along the second half of the Nera River section, this 1.2 km thick formation consists of interbedded siltstones and sandstones, coarse to fine-grained sandstones and polygenic breccias (Fig. 4) regrouped into FAm6, FAm5, FAm4, FAm3, FAm2 and FAm1 (Fig. 12). Sedimentary structures such as traction carpets are observed within FAm3 (Fig. 12b). Thick sandstone beds of FAm2 typically exhibit sharp to erosional basal surfaces with common rip-up clasts and sharp grain-size increases. Breccia facies, regrouped as facies association FAm1 comprise: (1) thin to medium-bedded, polygenic, faintly cross-laminated, clast-supported, well-sorted angular to subangular granule to pebble-sized breccias within a fine-grained sandstone matrix (Fig. 12c); (2) thin to medium-bedded, polygenic, erosional, anisopaceous, moderately sorted, matrix-supported, angular to subangular pebble-sized breccias displaying traction carpets and cross-bedding; (3) thick bedded, polygenic, poorly to moderately sorted, clast-supported, angular to subangular granule to cobble-sized breccias (Fig. 12d); (4) thick to very thick-bedded, polygenic, poorly sorted, matrix-supported, subangular to rounded, pebble to cobble-sized breccias within a medium to coarse-grained sandstone matrix and sparse sub-angular extraformational blocks (Fig. 12e). Outcropping conditions do not allow any clear facies trends or stacking patterns to be determined. However, through all the Upper Bourail Flysch Formation, an overall coarsening upward trend is observed, with a lower part comprised of FAm6, FAm5 and FAm4 with noticeable slope failures evidenced by clear truncations of beds along arcuate surfaces delimiting slumped intervals (Fig. 13a). The middle part is dominated by FAm3 to FAm1 with breccia facies interfingered within thick-bedded clinopyroxene-rich sandstones of FAm3 and FAm2. These erosive breccias vary laterally in thickness and form channelised decametre-long lenses (Fig. 13b). The upper part is organised as successive very thick-bedded polygenic breccia beds (FAm1) within a clinopyroxene-rich sandstone matrix.

4.2 Mineralogical composition

4.2.1 Petrographic results

Qualitative and quantitative petrographical analyses on thin sections are detailed in Appendix A. They reveal that the Gouaro Formation sandstones are mainly composed of quartz, feldspar, volcanic clasts and silicified mudrock clasts (Fig. 14a). Minor components comprise recrystallised (silicified) rounded biogenic debris (foraminifera, radiolaria and sponge spicules), as well as altered clinopyroxenes and metamorphic clasts. Coal clasts are also observed at the base of beds and pyrite concretions are present along very fine-grained fractions. In the "Mamelons Rouges Beds Formation", quartz, feldspar plagioclases and recrystallised planktonic foraminifera are the only components observed (Fig. 14a).

The increase in carbonate content within the Adio Limestone Formation is due to biogenic elements such as undifferentiated bioclasts, benthic and planktonic foraminifera, red algae, shell debris, sponge spicules, echinoids and bryozoans (Fig. 14b). Calcareous nannofossils are also sporadically present. The proportion of biogenic debris progressively increases up-section in favour of the siliciclastic phase (Fig. 8). The latter is represented by plagioclase, silicified mudstone clasts, quartz, chlorite, black opaques and volcanic clasts such as microlithic basalts. Additionally, fine to medium-grained, angular glauconite clasts are sparsely present.

The Lower Bourail Flysch Formation comprises abundant calcareous clasts and feldspar, while quartz and siliciclastic clasts are common (Fig. 14c). Up section, planktonic foraminifera remain very rare, but benthic foraminifera become common at the top of the formation at the expense of siliciclastic and calcareous clasts (Appendix A).

An increase of biogenic material is observed in the Middle Bourail Flysch Formation which is marked by a clear increase in biogenic debris within sandstone beds compared to the Lower Bourail Flysch. Benthic and planktonic foraminifera (Fig. 14d) are both present from rare to abundant, whereas biogenic debris such as bivalves, bryozoans, algae, echinoids and shells are common. Calcareous nannofossils are scarce. Biogenic components replace siliciclastic and calcareous lithoclasts, which are respectively abundant and common (Appendix A). On the contrary, silicified mudrock clasts become more abundant upward.

The Upper Bourail Flysch Formation is marked by a strong increase in clinopyroxenes, silicified mudrock clasts and calcareous clasts (Appendix A). While rare at the base of the formation, clinopyroxene becomes common to abundant further up the section (Fig. 14e; Appendix A). Silicified mudrock and calcareous clasts are commonly present. Inversely, siliciclastic clasts are abundant at the base of the formation, but their abundance decreases upward. On a macroscopic scale, the breccia clasts are composed of, in decreasing order of their relative abundance within the clasts: silicified mudrocks (Fig. 14e), micritic mudstones with planktonic foraminifera and siliceous nodules (Fig. 14e), sandstone and siltstone clasts, and foraminifera-rich, shell debris-rich bioclastic grainstone with red algae and coral fragments.

4.2.2 Hyperspectral results

The petrographic observations (Section 4.2.1) are supported by the hyperspectral results from the VNIR-SWIR and TIR domains. In the VNIR-SWIR domain, four main mineralogical groups are dominant: sulphates, carbonates, chlorites and white micas. In the Gouaro Formation, white micas are the dominant group (70 to 90%) present throughout the formation with a few intervals recording the presence of sulphate, associated with muddy intervals (FAm6) (Fig. 6). This association is also observed along the “Mamelons Rouges Beds Formation”, where a strong increase in the relative abundance of sulphate is observed (Fig. 4).

The sharp mineralogical change observed at the base of the Adio Limestone Formation is confirmed by hyperspectral data in the SWIR wavelength domain, with a progressive increase in carbonate (~20 to 80%) and a consistent relative abundance of white micas (~20%) (Fig. 8). In the Lower Bourail Flysch Formation, white micas, chlorite, and carbonates are present throughout the interval with a consistent relative abundance of approximately 60%, 20%, and 10%, respectively (Figs. 4, 10a). However, there is a constant relative abundance change at the bottom of the Middle Bourail Flysch Formation. From -705 m to ~-600 m, the relative abundance of white micas decreases in favour of carbonate. Here, only chlorite and carbonate are detected in the SWIR wavelength domain (Fig. 4).

In the TIR wavelength domain, silicates, sulphates, carbonates, chlorites, white micas and plagioclase are the main detected mineralogical groups (Fig. 4). In the Gouaro Formation, silicates are dominant throughout the formation (Fig. 6a). Carbonates and smectite are rare, while sulphates, chlorite and plagioclase abundances vary (0-50%; 20-40% and 5-50% respectively). Sandy intervals are marked by abundant silicates (quartz >50%) and feldspars (plagioclase >30%) whereas white micas and chlorite are the main components of muddy intervals (Fig. 6b). These differences are causally linked to variations in grain size and composition of the muddy matrix. In the "Mamelons Rouges Beds Formation" hyperspectral data record a decrease then an increase in the relative abundance of silicates in favour of sulphate (Fig. 4). In the Adio Limestone Formation, silicates progressively decrease through the section in favour of carbonates (Fig. 8). In addition, plagioclases are detected at the base of the section, in association with FAc3 and FAc2. The Lower Bourail Flysch Formation and Middle Bourail Flysch Formations are characterised by a consistent relative abundance of the silicate group (~40%) (Fig. 4). In the Lower Bourail Flysch Formation, sandstone beds are characterised by an increase of plagioclases and carbonates (Fig. 10). However, interbedded siltstones and very fine-grained sandstones are characterised by an increase of chlorite and white micas (Fig. 10b). In the Middle Bourail Flysch Formation, the relative abundance of chlorite increases from ~20 to ~40% at the expense of the carbonates (Fig. 4).

4.3 Palaeontological age determination

Throughout the studied section fossil preservation is poor with highly deformed and recrystallised foraminifera and calcareous nannofossils, due to the strong tectonisation and burial of these units during emplacement of the ophiolite. However, in the Gouaro Formation, undeformed Globotruncanidae foraminifera are present and *Globotruncanita* sp. is observed (in samples B355 and B339, respectively). The presence of these taxa suggests a late Cretaceous (Santonian to Maastrichtian) age for this formation (Robaszynski et al., 1984; Hornibrook et al., 1989). These foraminifera are also observed in the "Mamelons Rouges Beds Formation". Globotruncanidae are present (in samples B318 and B296) and suggest a late Cretaceous age for this formation.

New biostratigraphic data for the Adio Limestone Formation are based on planktic foraminifera and calcareous nannofossils. Planktic foraminifera species span the late Palaeocene to Early-Middle Eocene. In the basal part of the Adio Limestone Formation (samples B289, B287, B286), *Parasubbotina* cf. *varienta, Praemurica* sp. and *Subbotina* sp. are present and suggest a late Palaeocene (biozones P4 to E3) to Early Eocene (biozone E3) age (Fig. 8). The presence of *Subbotina senni, Morozovella lensiformis, Subbotina eocaena, Subbotina linaperta, Acarinina cuneicamerata* and *Acarinina bullbrooki* at the top of the formation, (samples B283, B282, B279) suggests an early to middle Eocene age (E6 – E13 biozones). Calcareous nannofossils are very rare in this interval but the presence of specimens ascribable to *Reticulofenestra* spp. in sample N292 indicates an age younger than the early Eocene (Fig. 8). The presence of a single specimen of *Reticulofenestra umbilicus* in sample N269 suggests a Lutetian age (Zone CNE13) (Agnini et al., 2014). This inconsistency between age determinations from calcareous nannofossils and foraminifera is likely due to the fact that foraminifera were identified in thin sections. Moreover, at the bottom of the formation, calcareous nannofossils indicate a younger age compared to planktonic foraminifera. Thus, we are more confident with age derived from calcareous nannofossils in that section. For this reason, and considering biostratigraphic data of overlying formations, we have tentatively assigned a middle Eocene age to the Adio Limestone.

The Lower Bourail Flysch age determination is divided into two parts. In the lower section, samples N268 to N263, calcareous nannofossil assemblages are characterised by the simultaneous presence of *R. umbilicus* and *Sphenolithus furcatolithoides* morphotype B and the absence of *Cribrocentrum reticulatum*, which suggest that this interval could be ascribed to mid-Lutetian (Zone CNE13). From sample N261 to the top of the LBF (sample N127) the presence of *C. reticulatum*, and *Dictyococcites bisectus* (> 10 µm) indicates a Bartonian age (Zones CNE15 - CNE16). Unfortunately, sphenoliths are rare in this succession so a careful approach is preferred, and the absence of *Sphenolithus obtusus* has not be used as an additional biostratigraphic constraint. The last occurrence of this taxon defines the base of Zone CNE16 thus the absence of this taxon could suggest that this interval can be ascribed to Zone CNE16. Ages indicated by the calcareous nannofossils are also confirmed by the presence of planktonic foraminifera *Acarinina primitiva* (sample B257) and *Pseudohastigerina wilcoxensis* (sample B238) which indicate a Lutetian age for this first interval, and a Bartonian age for the second interval due to the presence of *Turborotalia pomeroli* (sample B132) and *Turborotalia cerroazulensis* (sample B123).

At the base of the Middle Bourail Flysch Formation (sample N121) calcareous nannofossil assemblages are assigned to the undifferentiated Zones CNE15- CNE16 (i.e. Bartonian). Sample N109 can be ascribed to ealy Priabonian (Zone CNE17) based on the high abundance of *Cribrocentrum erbae*; the base of the acme of *C. erbae* is used to denote the base of the

Priabonian stage (Agnini et al., 2011). From sample N105 to sample NERA3, the calcareous nannofossil assemblage is characterised by the presence of *C. reticulatum* and the virtual absence of *C. erbae* indicating that this interval can be ascribed to a Priabonian age (Zones CNE18-CNE19). The presence of a single specimen of *Cribrocentrum isabellae* in sample NERA3 suggests that the base of Zone CNE19 may be identified with more detailed highly-resolved analyses. From sample N109, Palaeocene reworking progressively increases upward. Calcareous nannofossil biostratigraphic results are also supported by planktonic foraminifera data, with the presence of *Turborotalia cerroazulensis, Subbotina* cf. *gortanii* and *Turborotalia pomeroli* indicating a middle to late Eocene age in samples B76, B34 and B12. Moreover, an important reworking of Palaeocene species and contemporaneous shallow water species, such as *Nummulites* sp., *Discocyclina* sp., *Amphistegina* sp., or *Assilina* spp. is also observed in the foraminifera assemblages.

Along the top of the section, strong weathering of the rocks and poor outcropping conditions limit the number of samples from the Upper Bourail Flysch Formation. In addition, biogenic components are poorly preserved. This formation has not been biostratigraphically dated in this study. However, based on the structural position of the Upper Bourail Flysch Formation beneath the tectonic nappes, thought to be emplaced during the latest Eocene in the Nepoui region (Cluzel, 1998), the age of the top of this formation is speculated to be uppermost Priabonian.

4.4 Unit boundaries

Sedimentological, mineralogical, and palaeontological characteristics of each formation are used to determine and characterise boundaries between formations crossed by the CADART-1 / Nera River Section. The lowermost boundary crossed by the well corresponds to the limit between the Gouaro and “Mamelons Rouges Beds Formation”. This boundary is gradational, however, here we place it at -1720 m based on the loss of the prominent sandstone beds together with a strong increase in pyrite concretions and post-depositional gypsum mineralisation (Fig. 4). The top of the “Mamelons Rouges Beds Formation” corresponds to a highly deformed and fractured interval with centimetre-thick calcitic veins and tectonic breccia spanning -1617 m to -1615 m. Biostratigraphic data suggest that there is an important time gap between the Mamelons Rouges Beds and the Adio Limestone formations (see Section 4.3). Borehole data record a significant mud loss and a poor recovery rate at the top of this unit (France, 2000), which strongly suggests that a tectonic contact separated the two formations, as already noted by Maurizot and Cluzel (2014). The top of the Adio Limestone Formation is defined by a sharp reversal to siliciclastic lithologies and the occurrence of thick fractured intervals highlighted by calcitic veins. Biostratigraphic data suggest that there is a hiatus at the base of the Lower Bourail Flysch. Consequently, we also attribute the limit between these two formations as a tectonic contact, as noted by Maurizot and Cluzel (2014). Formation boundaries between Lower to Middle and Middle to Upper Bourail Flysch Formation are gradational and associated with progressive changes in mineralogical composition and sedimentary facies (Appendix A). The boundary between the Lower and Middle Bourail Flysch is marked by a compositional change from siliciclastic to calcareous sandstones. This transition is clearly visible on hyperspectral data and based on these, the boundary was inferred to be at -711.5 m. The top of the Middle Bourail Flysch Formation is marked by an increase in clinopyroxenes in the lithic phase of sandstones (Appendix A) and, although gradational, has been set at +605 m. Finally, the top of the Nera River section is marked by a tectonic contact between the Upper Bourail Flysch Formation and a tectonic slice of Sedimentary Basement overlain by the Poya Nappe (Fig. 3). On the western part of the

Bourail Anticline, this thrusted contact is observed with the Montagnes Blanches Nappe and a tectonic slice of Sedimentary Basement.

5. Discussion

5.1 Depositional environmental interpretation

All of the formations described in this study are believed to have been deposited within deepwater environments, yet no specific palaeobathymetric depth is identified. Facies associations point to depositional processes from (hemi)pelagic suspension fallout or submarine gravity flows in deepwater settings (see Table 1). The bedded character of the Gouaro Formation, the preservation of bed tops, together with the lack of clearly erosional, disconformable surfaces and cross-bedding suggest that deposition of the Gouaro Formation occurred within a poorly channelised turbidite fan made of sheet-like or lobate basin floor deposits (Galloway, 1998; Mulder and Etienne, 2010; Liu et al., 2018). However, the occurrence of conglomeratic deposits could suggest catastrophic slope or shelf edge destabilisation events or, alternatively, sediment by-pass (Kastens and Shor, 1985; Wuellner and James, 1989). Massive siltstones facies from hemipelagic decantation present in the "Mamelons Rouges Beds Formation" let us to interpret an hemipelagic basin plain.

The sedimentary facies of the Adio Limestone Formation and its paleontological content with benthic foraminifers and biogenic debris from middle to external platform environments reworked with bathyal planktonic foraminifers and calcareous nannofossils strongly suggest reworking into deepwater environments by gravity flow processes. This formation is thus seen as reflecting hemipelagic to pelagic deepwater sedimentation in open marine settings, supplemented by significant gravity flow inputs from a coeval shallow water carbonate platform(s) and local slope destabilisations.

Similarly to the Gouaro Formation, the sedimentary facies, stacking patterns and depositional hierarchy following nested depositional cycles of the Lower Bourail Flysch Formation is seen as reflecting deposition within a basin floor fan made of unchannelised depositional lobes (Mulder and Etienne, 2010). However, the occurrence of amalgamation surfaces with common mudclasts, together with sharp grain size breaks could suggest some degree of bypass and/or channelling, possibly as individual channels within lobe axis settings.

The isopaceous and tabular geometry of the Middle Bourail Flysch, organised as metre-thick asymmetric sequences suggest progradational or compensational stacking of lobes (Mutti and Sonnino, 1981; Pickering et al., 1989) possibly following a reduction in the sedimentation rate / depocenter space ratio (Liu et al., 2018). This is consistent with a period of carbonate platform development and drowning which would imply a relative shutdown in clastic fluxes during the Priabonian (see Section 5.2).

Finally, the lenticular breccia of the Upper Bourail Flysch Formation, suggest deposition after a short-transport distance, possibly as base-of-slope aprons (Richards et al., 1998) which are typified by a weak longitudinal extent.

5.2 Sedimentary sources

The petrographic and hyperspectral analyses performed in this study provide information on the relative abundance variations of all the components identified in the late Cretaceous to Palaeogene sediments of the Gouaro Anticline. Relative abundances of these components and their evolution through the section allow us to discuss the potential sources that fed the

Bourail Basin and how these sources changed over time. Four different groups of components are discussed (1) quartz and feldspar, (2) biogenic debris, (3) sedimentary lithics with silicified mudrock, calcareous and siliciclastic clasts and (4) clinopyroxenes, whose nature, relative abundances and evolution are diagnostic and are used to identify sediment sources and their evolution.

5.2.1 Quartz and feldspar: permanent siliciclastic input from syn-rift and basement units

Quartz and feldspar are present throughout the section from the late Cretaceous to the late Eocene. Quartz has a relatively constant abundance (TIR results, Fig. 4) while feldspars are present in sandstone beds (Fig. 4). This consistency from the late Cretaceous suggests that they were derived from a long-term subaerial source and/or from marine reworking of contemporaneous and older formations to those studied here. The quartz component identified in the Lower Bourail Flysch Formation could be fed by reworking from: (i) the syn-rift siliciclastic Formation à Charbon; (ii) the Pic Jacob Formation which corresponds to syn-rift volcanism (Cluzel et al., 2010; Nicholson et al., 2011; Maurizot et al., 2020a); and/or (iii) older sedimentary basement units.

5.2.2 Biogenic debris: middle to late Eocene shallow water carbonate platforms

The reworking of shallow water biogenic components such as benthic foraminifera, shell and bivalve debris, bryozoan and other elements (sponge spicules, coral clasts, etc.) are mainly observed in the Lutetian Adio Limestone and middle to late Eocene Middle Bourail Flysch Formation. The contemporaneous reworking and/or erosion of shallow water carbonate is highlighted by the presence of shallow water benthic foraminifers species *Amphistegina sp, Discocyclina sp, Assilina sp, Rotaliidae and Nummulites sp*, (Boudagher-Fadel, 2008). In both formations, these faunas reworked from the shallow water domain have the same ages as the pelagic nannofossils. This suggests that a shallow water carbonate platform was present during the deposition of these gravity systems. Of particular note is the presence of an *in-situ* shallow water carbonate platform of middle to late Eocene age in the Uitoé area (Fig. 1), recorded by the Bartonian to Priabonian Uitoé Limestones, which rest unconformably on the sedimentary basement (Maurizot, 2014). Such shallow water carbonates could be the remnants of the platform that fed the Middle Bourail Flysch Formation, as supported by the similar ages and faunal taxa found in the Middle Bourail Flysch Formation. The older Lutetian Adio Limestone Formation contains shallow water components but is interpreted as deepwater turbidite limestones and has no known associated contemporaneous shallow water carbonate formation. Thus, the presence of reworked and hemipelagic fauna of the same age infers a contemporaneous filling of the Bourail Basin.

5.2.3 Sedimentary lithics: reworking of the post-rift cover

Clasts of silicified mudrock and calcareous rocks (typically micritic mudstone) are the dominant sedimentary lithic components within the Bourail Group. These clasts are most likely present due to the erosion of Upper Cretaceous to Eocene post-rift deepwater deposits. Silicified mudrock and micritic mudstone clasts could be respectively linked to the Black Chert Formation and the *Globigerina* Limestone and/or Adio Limestone formations, as proposed in Maurizot and Cluzel (2014). Previous work has shown that the Black Chert facies are only observed in the Black Chert Formation (Routhier, 1953; Maurizot, 2011) and that the only New Caledonian geological formations which are composed of micritic mudstone correspond to the Former Adio Limestone Formation (Routhier, 1953; Gonord, 1977; Paris, 1981; Maurizot, 2012) and the *Globigerina* Limestone (Paris, 1981; Maurizot, 2011).

Other siliciclastic clasts (green chert, metamorphic clasts) and calcareous clasts, such as grainstone blocks observed in the Upper Bourail Flysch Formation, are less diagnostic. Many potential sources could be identified and they could be derived from several formations, such as the Lower Bourail Flysch Formation, Gouaro Formation, Formation à Charbon as well as the Uitoé Limestones. In the breccia of the Upper Bourail Flysch Formation, the angularity of most of the clasts (black chert, micritic mudstone, grainstone blocks) imply a relatively short distance for transportation, which would suggest that these clasts are derived from a different location than the quartz and feldspars and the sand-sized fraction of the clinopyroxene rich sandstone.

5.2.4 Clinopyroxenes: an input from the Poya Nappe?

The appearance and progressive upward increase in the abundance of clinopyroxenes is a distinct compositional change through the Upper Bourail Flysch Formation (Appendix A). Maurizot and Cluzel (2014) identified that these minerals plot in the field of EMORB basalts and suggest that they were derived from the Poya Nappe that comprises E-MORB basalts. This interpretation is suggested as the Poya Nappe is mainly composed of a basalt with a MORB signature which could be the origin of the Upper Bourail Flysch Formation clinopyroxene (Maurizot and Cluzel., 2014; Maurizot et al., 2020b). However, the formation of such fine-grained sands found within the Upper Bourail Flysch Formation, implies a subaerial exposure of the Poya Nappe during the late Eocene, which is hardly reconciled when considering the very likely subaqueous settings of such an obducted oceanic crust nappe. Moreover, the lack of materials derived from the other rocks comprised in the Poya Nappe (such as abyssal red cherts, radiolarites, turbidite sandstones or dolerites) and the absence of coarser reworked material of oceanic origin, both in the sandstone matrix and breccia, questions the link between the Upper Bourail Flysch Formation and the Poya Nappe. In addition, the recently identified Eocene volcanic chain along the western flank of Norfolk Ridge (Mortimer et al., 2020) also evidenced by Priabonian volcaniclastic turbidites at site IODP Site U1507 located in the New Caledonia Basin at the foot of one of the Norfolk Ridge volcano (Sutherland et al., 2019) could be an alternative source supplying the volcanic material found in the Upper Bourail Flysch. However, published geochemical data from the Eocene volcanoes (Mortimer et al., 2020) do not clearly indicate a MORB signature. Finally, the Koh Ophiolite (Meffre, 1995; Meffre et al., 1996) present in the New Caledonia basement composed of dolerites, boninites, gabbbros and pillow-lava with a MORB or BABB type basalt signature cannot be ruled out as a potential source. Thus, we believe that three potential sources could have provided the volcaniclastic material of the Upper Bourail Flysch but our dataset cannot favour one more than another.

5.3 Bourail Basin evolution

Along with sediment source variability, the compositional and facies changes observed throughout the Bourail Basin fill can help determine the main phases of basin development with a focus on platform-to-basin relationships and vertical motions. Deposition in deepwater basins is thought to directly record the variations of the feeding systems on the shelf (e.g., source variations, augmentation of sedimentary fluxes), which are controlled by relative sea level fluctuations (e.g., tectonic, palaeoclimatic) (Stow et al., 1984; Weber and Reilly, 2018). Our detailed characterisation shows that besides the overall coarsening and thickening upward trend observed throughout the succession, distinct and repeated intervals of siliciclastic-dominated (Gouaro, “Mamelons Rouges Beds Formation”, Lower and Upper Bourail Flysch Formation) *vs* carbonate-dominated (Adio Limestone Formation, Middle Bourail Flysch Formation) resedimentation occur (Appendix A). Carbonate-dominated intervals are considered to reflect phases of shallow water carbonate platform development, possibly marking drowning during subsidence phases or, alternatively, palaeogeographical or palaeoclimatic changes. On the other hand, siliciclastic-dominated intervals likely reflect periods of increased terrigenous inputs during base level drops, possibly as a result of tectonic uplifts. More precisely, we propose that the vertical evolution of the succession can be summarised in five main phases: (i) a late Cretaceous phase of siliciclastic sedimentation related to active rifting and associated horsts erosion (Gouaro Formation); (ii) a latest Cretaceous to middle Eocene (Lutetian) subsidence phase recorded by the progressive onset of pelagic and resedimented carbonates ("Mamelons Rouges Beds" and Adio Limestone formations); (iii) a Lutetian to Bartonian renewal in terrigenous fluxes, recorded by the deposition of a thick siliciclastic turbidite fan (Lower Bourail Flysch Formation), possibly associated with an uplift, (iv) a second drowning phase in the Priabonian, recorded by calciturbidites in the basin (Middle Bourail Flysch Formation) and shallow water carbonates on the Norfolk Ridge (e.g., Uitoé Limestones); and (v) a poorly dated Priabonian to post-Eocene phase of substantial volcaniclastic/siliciclastic inputs and submarine slope destabilisations (Upper Bourail Flysch Formation), possibly associated with a second uplift and regional volcanism. The possible origins of this polyphased evolution are discussed in the following sections.

5.3.1 Deepwater sedimentation during late Cretaceous rifting

The Gouaro Formation corresponds to the first siliciclastic-dominated interval. On the basis of our depositional processes and environmental interpretations, this Santonian/Maastrichtian formation is thought to record deposition within a poorly confined turbiditic environment. This suggests the existence of deepwater basins on or in the vicinity of the Norfolk Ridge during the late Cretaceous, the infill of which being coeval with the paralic Cenomanian/Campanian “Formation à Charbon” (Maurizot et al., 2020a). The Gouaro Formation sandstones, composed of quartz, feldspar and sedimentary and volcanic lithics, may correspond to a distal equivalent of the deltaic sandstones of the “Formation à Charbon”, as supported by similarities with regards to age, mineralogical components and also by the presence of coal in turbidite beds. The “Formation à Charbon” is mainly composed of quartz, plagioclase, lithic elements (andesite, trachyte and rhyolite) and coal layers (Paris, 1981; Cluzel et al., 2011; Maurizot et al., 2020a). These two-coeval formations suggest a complete sedimentary system from deltaic sandstones, fed by a contemporaneous alkaline volcanism and erosion of sedimentary basement, to poorly confined deepwater turbidites. The late Cretaceous age of these two-coeval formations corresponds regionally to the widespread rifting of the eastern margin of the Gondwana continent (Gaina et al., 1998; Crawford et al., 2003; Sdrolias et al., 2003; Schellart et al., 2006; Whattam et al., 2008; Collot et al., 2020). The siliciclastic formation of the “Formation à Charbon” is considered to record this extensive phase (Paris, 1981; Cluzel et al., 2011, 2012; Maurizot et al., 2020a). The Gouaro Formation is also associated to the late Cretaceous rifting stage and the short distance between this formation and its coeval deltaic sandstones in the Bourail area (less than 12 km) (Fig. 3) could result from an important shortening of all the sedimentary pile, also supported by the numerous reverse faults and tectonic contact present in the area (Espirat, 1971; Gonord, 1977; Paris, 1981).

5.3.2 Uppermost Cretaceous subsidence

In New Caledonia, the upper Cretaceous Mamelons Rouges Beds Formation and the overlying upper Cretaceous to Palaeocene Black Chert Formation conformably overlie all syn-rift formations. They are interpreted to record a generalised drowning leading to a deepening and widespread blanketing of all sedimentary basins. This palaeogeographic “homogenisation” is seen as reflecting post-rift thermal subsidence during the deposition of the “Mamelons Rouges Beds Formation” and Black Chert Formation (Maurizot et al., 2020a). The lack of the latter in the CADART-1 / Nera River section could be explained by the tectonic contact observed at -1614 m (Fig. 4). This hiatus between “Mamelons Rouges Beds Formation” and Adio Limestone, including the whole Palaeocene, could be the result of this tectonic contact, as suggested by the important fracturation of the corresponding interval.

5.3.3 Lutetian basin reorganisation or continued post-rift thermal subsidence?

The Gouaro and Mamelons Rouges Beds marginal to deepwater, siliciclastic-dominated deposits are progressively overlain by a calcareous-dominated interval with pelagic limestones and calciturbidites during the lower and middle Eocene. This is recorded by the *Globigerina* Limestone, the Adio Limestone and the Creek Aymes Limestone formations. In the CADART-1 well, this contact is interpreted to be tectonic, induced by post-deposit thrust linked to the onset of the ophiolitic complex onto Grande Terre.

The presence of frequent glauconite clasts, biogenic debris, and shallow water fauna (Section 4.2) in the Adio Limestone Formation is indicative of a low energy depositional environment and low sedimentation rates, allowing the development of these iron oxides (Föllmi, 1996; Flügel, 2013). These carbonate deposits show basin reorganisation with the development of a shallow water carbonate platform and their reworking deposited in a deepwater environment as calciturbidite beds.

Three scenarios could explain this palaeogeographic setting. The first, following interpretation of Maurizot and Cluzel (2014), is to propose that the Adio Limestone corresponds to the first record of tectonic activity linked to convergence phases, starting at 55 Ma around Koumac, following Cluzel et al. (2006), who attributed subduction related boninitic dykes to the onset of the South Loyalty subduction. Maurizot and Cluzel (2014) propose that these limestones would be the first record of convergence, being deposited on the forebulge domain of the flexural basin associated with the South-Loyalty subduction.

A second scenario could be that the Adio Limestone Formation are deposited in the continuity of the post-rift thermal subsidence. Such sustained subsidence would lead to the progressive drowning of nearby rift-related topographic highs where shallow water carbonate platforms could eventually develop and feed adjacent deepwater basins. Long post-rift subsidence phases associated with a shift in sedimentation from siliciclastic to carbonates are known in other margins and sedimentary basins such as those of the Grand Banks region (Quebec offshore domain). In this area, a long thermal subsidence (Early to Late Jurassic) is marked by the siliciclastic Downing and Voyager Formation (siltstone and marls) overlain by calcareous Rankin Formation (McAlpine, 1990; Driscoll et al., 1995).

Finally, a third scenario where the shift to carbonate sedimentation is controlled by palaeoclimatic and/or palaeogeographic changes without invoking any substantial subsidence/uplift vertical motions, cannot be ruled out. The Palaeocene to early Eocene was an interval of significant palaeoclimatological change, with global records of decreasing $\delta^{18}O$ through the Palaeocene suggesting increasing global temperatures with a peak during the early Eocene (Zachos et al., 2001, 2008) and global sea level curves suggesting an overall increase in global sea level through the late Palaeocene to middle Eocene (Miller et al., 2005). These global variations favour an increase in calcareous production. Palaeogeographically, the South-West Pacific observed a change in plate-motion between the Ypresian to Lutetian, with a northward translation (Breton et al., 2004; O'Connor et al., 2013). This event drove the Zealandia continent to a higher palaeolatitude (40° to 20°S) (Sdrolias et al., 2003; Schellart et al., 2006) which would impact sedimentation, from siliclastic to calcareous-dominated. Furthermore, in New Zealand a very similar shift occurs in the Late Palaeocene from the cherty Whangai Formations to the Amuri Limestones (Hancock et al., 2003; Hollis et al., 2005; Hollis, 2007; Dallanave et al., 2015; Slotnick et al., 2015) and is attributed to a global warming event.

Thus, the onset of the Adio Limestones Formation could be interpreted as a record of (i) a tectonic event which reorganised palaeogeography with new high and low domains; or (ii) shelf drowning along a post-rift thermal subsidence where flooding of siliciclastic system allowed carbonate platform development; or (iii) where palaeoclimate and latitude permit a shift from siliciclastic to carbonate sedimentation without a relative sea-level drop. In comparison with New Zealand's geological history, the lack of clastic supply associated with tectonic uplift, global warming and palaeolatitude variations of the Zealandia continent, suggests one of the last two scenarios, with high and deep domains corresponding to inherited structures from the rifting period.

5.3.4 Middle Eocene uplift

The conformable but strongly tectonised upper boundary of the Adio Limestone Formation in the CADART-1 well is overlain by the 801 m thick Middle Eocene Lower Bourail Flysch Formation succession that is composed of siliciclastic turbidites whose sources are interpreted to come from the basement, mixed with components from Cretaceous to Palaeocene sedimentary cover (Section 5.2.1). This renewal of terrigenous input in the Bourail Basin constitutes an important change in sedimentary environment that we interpret as being related to an uplift. The Lutetian to Bartonian age of the Lower Bourail Flysch Formation indicates that this uplift is contemporaneous with the recently dated transition in the Noumea area, from pelagic *Globigerina* Limestone to hematite rich pink calciturbidites, interpreted as resulting from an uplift and erosion of the Norfolk Ridge (Dallanave et al., 2018).

The middle Eocene is also a critical time in northeastern New Caledonia where the peak of high pressure low temperature metamorphism occurs at 44 Ma, which records the deepest burial of rocks down to ca. 80 km depth and hence the onset of their exhumation from 44 Ma to 34 Ma (Baldwin et al., 2007). At a regional scale, recent studies based on the analysis of marine geological data have documented the 'Tectonic Event of the Cenozoic in the Tasman Area', an Eocene episode of widespread compression and uplift of the ridges of northern Zealandia that is thought to be responsible for the major middle Eocene to Oligocene unconformity observed in the DSDP and IODP wells of the LHR (Burns et al., 1973; Collot et al., 2008; Sutherland et al., 2010, 2017, 2018; Bache et al., 2012; Etienne et al., 2018). This regional tectonic event and associated uplift are linked to the Tonga-Kermadec subduction initiation along the eastern part of Zealandia Continent during the Eocene (Sutherland et al., 2017, 2020).

According to these local to regional observations, we suggest that the middle Eocene uplift of the Norfolk Ridge, responsible for the deposition of the Lower Bourail Flysch, is the result of a tectonic event likely to be associated with New Caledonian metamorphic complex activity or subduction initiation observed regionally.

5.3.5 Bartonian to Priabonian drowning

The transition between the siliciclastic-dominated deposits of Lower Bourail Flysch and the calcareous-dominated Middle Bourail Flysch Formation is interpreted to reflect a transgressive phase associated to a general flooding. Indeed, the proportion of quartz, feldspar and sedimentary lithics progressively decreases in favour of biogenic debris and foraminifera.

Benthic foraminifera identified in the Middle Bourail Flysch Formation indicate the nearby development of a shallow water carbonate platform. As previously suggested, because of its shallow water character, its nearby position and its contemporaneous age, the Uitoé Limestones, that directly overlie the sedimentary basement, are very good candidates for the carbonate source of the Middle Bourail Flysch succession.

The Middle to Late Eocene period is characterised by a regional cooling (Zachos et al., 2001, 2008) and fall of sea level (Miller et al., 2005). These two trends are not in favour of a development of carbonate platform. Hence we interpret the deposition of Middle Bourail Flysch Formation as being related to a second phase of drowning of the Norfolk Ridge. The origin of this second drowning period is not clearly identified. Previously interpreted as the deepening of the forebulge domain (Maurizot, 2014; Maurizot and Cluzel, 2014), other local and regional tectonic events could be linked to this period. As the first tectonic uplift, this drowning phase could be also linked to metamorphic complex exhumation which occurred between 44 to 38 Ma (Baldwin et al., 2007). Metamorphic complex exhumations are generally assumed to occur during extensive regimes (Davis and Coney, 1979; Coney, 1980; Wernicke, 1981; Tirel et al., 2004, 2008), in different geodynamical settings as post-collisional extension (Wernicke and Burchfiel, 1982; Wernicke, 1985; Davis et al., 1986) and/or slab-roll back extension (Le Pichon et al., 1981; Jolivet et al., 2009). New Caledonian metamorphic complex exhumation linked to an extensive regime could be responsible for the drowning phase.

5.3.6 Late Eocene to Oligocene? uplift and origin of breccias

The Upper Bourail Flysch Formation is 1.2 km thick and is poorly dated. The basal 700 m of the formation are exclusively composed of clinopyroxene rich sandstones interpreted by

Maurizot and Cluzel (2014) to be sourced from distal erosion of basalts (Section 5.1) and the top 500 m are alternations of clinopyroxene rich sandstones and polygenic breccias that show an overall coarsening and thickening upward sequence.

Our observations show that the onset of these breccias, interpreted as debris flows, likely denotes a substantial change in slope values. The angularity and size of elements, the short lateral extension of beds, the normal grading and amalgamated surfaces supported by clast-supported basal lags indicate a short transport distance of these breccias which corroborates the slope destabilisation interpretation (Courjault et al., 2011; Ferry et al., 2015). Major slump surfaces associated with the breccias and soft sediment deformation such as folds also corroborate this interpretation. It has been shown that slope breaks located at the mouth of canyons or gullies can generate a hydraulic jump that leads to the deposition of breccia lobes, mega-ripples and inclined stratification. Hence we suggest that the Bourail Basin breccias could be formed in a similar context at the base of a slope in reaction to a very proximal slope increase and destabilisation. Festa et al. (2016) also show that breccias and olistoliths could be linked to many diverse tectonic settings, from rift-drift and passive margin to convergent margin as subduction, obduction or collisional environment. Maurizot and Cluzel (2014) proposed that the breccias were generated directly by the emplacement of the Montagnes Blanche Nappe. The onset of the latter would be responsible for slope increase and intraformational erosion would fed breccia beds present in the Upper Bourail Flysch Formation. However, the lack of clasts provided by the Poya and Peridotite nappes leads us to propose an alternative model. The latter would be based on a slope increase of the eastern domain of the Bourail Basin resulting from a general convergence phase. Interfingered with this breccia, derived from slope collapse, clinopyroxene rich sandstone could be from a distal part of the source system from Sedimentary Basement erosion, Norfolk Ridge Eocene

Volcanism or Poya Nappe, even if for these last two hypotheses, the clinopyroxene source is contentious and it is difficult to explain the sedimentological process of this fine-grained clinopyroxene rich sandstone in a subaqueous setting.

6. Conclusion

This detailed sedimentological description and sedimentary source analysis of the CADART-1 / Nera River section can be summarised as follows:

1. The Bourail Basin corresponds to a deepwater basin, filled with turbidite sandstone, as early as the upper Cretaceous. Identification of numerous tectonic contacts within the sedimentary section and rapid lateral variations of facies (e.g. deltaic sandstones in the Moindou area and the deepwater character of CADART-1) questions the degree of allochthony of the sedimentary units from the West coast of Grande Terre.
2. The upper Cretaceous to Palaeogene interval is fed by multiple sediment sources whose relative abundance shows important variations with time: (i) pre-existing sedimentary units (sedimentary basement); (ii) contemporaneous carbonate platforms; (iii) upper Cretaceous/Eocene sedimentary cover; and (iv) eroded volcanic rocks of which their origins are discussed.
3. We provide evidence for several significant phases of subsidence and uplift. While the uppermost Eocene evolution is very likely the result of pre-obduction sedimentary nappe emplacement, the other phases could result from other local tectonic events linked to metamorphic complex history, regional Tectonic Event of Cenozoic in the Tasman Area (TECTA as of Sutherland et al. (2017)), or palaeoclimatic events as observed in New Zealand.

4. We also discuss the mechanism for the origin of the breccias and their syn-tectonic character. Their organisation and reworked components do not allow us to link these breccias to the sedimentary nappe emplacement and could be linked instead to margin slope-increase which favours dissection of previous sedimentary cover.

This study builds a new framework of the Late Cretaceous – Eocene sedimentary units present in New Caledonia and proposes new alternatives for tectono-sedimentary evolution of the Bourail Basin region. Notably, according to this new interpretation of the sedimentary record of the Bourail Basin, effects of the convergence in Northern Zealandia are not showing up before Lutetian and even maybe as late as Priabonian, which implies a fast transition from collision to obduction..

Acknowledgements

The authors wish to thank Pierre Maurizot for his contribution on field indications and discussions concerning New Caledonia's geological history. Cherry Newsam is thanked for her English editing. Fieldwork and A. Bordenave's PhD were managed by the Geological Survey of New Caledonia, ADECAL Technopole and EA 4592 Georessource & Environment and funded by TOTAL. We also thank editor Catherine Chagué, and reviews from Alastair H.F. Robertson and Emmanuelle Chanvry, for their constructive comments that greatly improved the manuscript.

Reference list

Agnini, C., Fornaciari, E., Giusberti, L., Grandesso, P., Lanci, L., Luciani, V., Muttoni, G., Pälike, H., Rio, D., Spofforth, D.J.A., Stefani, C., 2011. Integrated biomagnetostratigraphy of the Alano section (NE Italy): A proposal for defining the middle-late Eocene boundary. GSA Bulletin 123, 841–872.

Agnini, C., Fornaciari, E., Raffi, I., Catanzariti, R., Pälike, H., Backman, J., Rio, D., 2014. Biozonation and biochronology of Paleogene calcareous nannofossils from low and middle latitudes. Newsletters on Stratigraphy 47, 131–181.

Aitchison, J.C., Meffre, S., 1992. New Caledonia a tectonic collage in the Southwest Pacific. 29th International Geological Congress, Kyoto, Japan, pp. 255.

Aitchison, J.C., Clarke, G.L., Meffre, S., Cluzel, D., 1995. Eocene arc-continent collision in New Caledonia and implications for regional southwest Pacific tectonic evolution. Geology 23, 161–164.

Aitchison, J.C., Ireland, T.R., Clarke, G.L., Cluzel, D., Davis, A.M., Meffre, S., 1998. Regional implications of U/Pb SHRIMP age constraints on the tectonic evolution of New Caledonia. Tectonophysics 299, 333–343.

Aubry, M.-P., 1984. Handbook of Cenozoic Calcareous Nannoplankton. Book 1: Ortholithae (Discoasters). Micropaleontology Press, American Museum of Natural History, New York, 266 pp.

Aubry, M.-P., 1988. Handbook of Cenozoic Calcareous Nannoplankton. Book 2: Ortholithae (Catinasters, Ceratoliths, Rhabdoliths). Micropaleontology Press, American Museum of Natural History, New York, 279 pp.

Aubry, M.-P., 1989. Handbook of Cenozoic Calcareous Nannoplankton. Book 3: Ortholithae (Pentaliths, and others), Heliotithae (Fasciculiths, Sphenoliths and others). Micropaleontology Press, American Museum of Natural History, New York, 279 pp.

Aubry, M.-P., 1990. Handbook of Cenozoic Calcareous Nannoplankton. Book 4: Heliolithae (Helicoliths, Cribriliths, Lopadoliths and others). Micropaleontology Press, American Museum of Natural History, New York, 381 pp.

Aubry, M.-P., 1999. Handbook of Cenozoic calcareous nannoplankton. Book 5: Heliolithae (Zygoliths and Rhabdoliths). Micropaleontology Press, American Museum of Natural History, New York, 368 pp.

Auzende, J.M., Rissen, J.P., Lafoy, Y., Gente, P., Charlou, J.L., 1988. Seafloor spreading in the North Fiji Basin (Southwest Pacific). Tectonophysics 146, 317–352.

Avias, J., 1967. Overthrust structure of the main ultrabasic New Caledonian massives. Tectonophysics 4, 531–541.

Bache, F., Sutherland, R., Stagpoole, V., Herzer, R., Collot, J., Rouillard, P., 2012. Stratigraphy of the southern Norfolk Ridge and the Reinga Basin: A record of initiation of Tonga–Kermadec–Northland subduction in the southwest Pacific. Earth and Planetary Science Letters 321–322, 41–53.

Baldwin, S.L., Rawling, T., Fitzgerald, P.G., 2007. Thermochronology of the New Caledonian high-pressure terrane: Implications for middle Tertiary plate boundary processes in the southwest Pacific. In: Cloos, M., Carlson, W.D., Gilbert, M.C., Liou, J.G., Sorensen, S.S. (Eds.), Convergent Margin Terranes and Associated Regions: A Tribute to W.G. Ernst. Geological Society of America, pp. 117–134.

Berggren, W.A., Pearson, P.N., 2005. A revised tropical to subtropical Paleogene planktonic foraminiferal zonation. Journal of Foraminiferal Research 35, 279–298.

Boudagher-Fadel, M.K., 2008. The Cenozoic larger benthic foraminifera: the Palaeogene. In: Boudagher-Fadel, M.K. (Ed.), Developments in Palaeontology and Stratigraphy. Elsevier, pp. 297–545.

Boudier, F., Nicolas, A., 2020. Semail ophiolite emplacement: a consensual mode? International Conference on Ophiolites and the Oceanic Lithosphere: Results of the Oman Drilling Project and Related Research. Sultan Qaboos University, Muscat, Sultanate of Oman, pp. 1-3.

Bouma, A.H., 1962. Sedimentology of Some Flysch Deposits: A Graphic Approach to Facies Interpretation. Elsevier, Amsterdam, Netherlands, 168 pp.

Bown, P., Young, J., 1998. Techniques. In: Bown, P. (Ed.), Calcareous Nannofossil Biostratigraphy. Chapman and Hall; Kluwer Academic, pp. 16–28.

Bown, P.R., 2005. Palaeogene calcareous nannofossils from the Kilwa and Lindi areas of coastal Tanzania (Tanzania Drilling Project Sites 1 to 10, 2003-4). Journal of Nannoplankton Research 27, 21–95.

Breton, J.-P., Béchennec, F., Le Métour, J., Moen-Maurel, L., Razin, P., 2004. Eoalpine (Cretaceous) evolution of the Oman Tethyan continental margin: insights from a structural field study in Jabal Akhdar (Oman Mountains). GeoArabia 9, 41–58.

Burns, R.E., Andrews, J.E., 1973. Site 208. Initial Reports of the Deep Sea Drilling Project, 21. US Government Printing Office, Washington, DC, pp. 271–331.

Chardon, D., Chevillotte, V., 2006. Morphotectonic evolution of the New Caledonia ridge (Pacific Southwest) from post-obduction tectonosedimentary record. Tectonophysics 420, 473–491.

Clark, R.N., King, T.V.V., Klejwa, M., Swayze, G.A., Vergo, N., 1990. High spectral resolution reflectance spectroscopy of minerals. Journal of Geophysical Research: Solid Earth 95, 12653–12680.

Cluzel, D., 1998. Le flysch post-obduction de Népoui, un bassin transporté ? Conséquences sur l'âge et les modalités de l'obduction tertiaire en Nouvelle-Calédonie (Pacifique sud-ouest). Comptes Rendus de l'Académie des Sciences, Séries IIA 327, 419–424. (in French)

Cluzel, D., Meffre, S., 2002. L’unité de la Boghen (Nouvelle-Calédonie, Pacifique sud-ouest) : un complexe d’accrétion jurassique. Données radiochronologiques préliminaires U-Pb sur les zircons détritiques. Comptes Rendus Géoscience 334, 867–874. (in French)

Cluzel, D., Picard, C., Aitchison, J.C., Laporte, C., Meffre, S., Parat, F., 1997. La Nappe de Poya (ex. formation des Basaltes) de Nouvelle Calédonie (Pacifique Sud-Ouest) : un plateau océanique campanien-paléocène supérieur obducté à l’Eocène supérieur. Comptes Rendus de l’Académie des Sciences, Paris 324, 443–451. (in French)

Cluzel, D., Chiron, D., Courme, M.-D., 1998. Discordance de l’Éocène supérieur et événements pré-obduction en Nouvelle-Calédonie. Comptes Rendus de l’Académie des Sciences - Séries IIA - Earth and Planetary Science 327, 485–491. (in French)

Cluzel, D., Aitchison, J.C., Picard, C., 2001. Tectonic accretion and underplating of mafic terranes in the Late Eocene intraoceanic fore-arc of New Caledonia (Southwest Pacific): geodynamic implications. Tectonophysics 340, 23–59.

Cluzel, D., Bosch, D., Paquette, J.-L., Lemennicier, Y., Montjoie, P., Ménot, R.-P., 2005, Late Oligocene post-obduction granitoids of New Caledonia: A case for reactivated subduction and slab break-off. Island Arc 14, 254-271

Cluzel, D., Meffre, S., Maurizot, P., Crawford, A.J., 2006. Earliest Eocene (53 Ma) convergence in the Southwest Pacific: evidence from pre-obduction dikes in the ophiolite of New Caledonia. Terra Nova 18, 395–402.

Cluzel, D., Adams, C.J., Meffre, S., Campbell, H., Maurizot, P., 2010. Discovery of Early Cretaceous rocks in New Caledonia: new geochemical and U-Pb zircon age constraints on the transition from subduction to marginal breakup in the southwest Pacific. The Journal of Geology 118, 381–397.

Cluzel, D., Adams, C.J., Maurizot, P., Meffre, S., 2011. Detrital zircon records of Late Cretaceous syn-rift sedimentary sequences of New Caledonia: An Australian provenance questioned. Tectonophysics 501, 17–27.

Cluzel, D., Maurizot, P., Collot, J., Sevin, B., 2012. An outline of the geology of New Caledonia; from Permian-Mesozoic southeast Gondwanaland active margin to Cenozoic obduction and supergene evolution. Episodes 35, 72-86.

Cluzel, D., Whitten, M., Meffre, S., Aitchison, J.C., Maurizot, P., 2018. A reappraisal of the Poya Terrane (New Caledonia): accreted Late Cretaceous-Paleocene marginal basin upper crust, passive margin sediments, and Early Eocene E-MORB sill complex. Tectonics 37, 48–70.

Cluzel, D., Boulvais, P., Iseppi, M., Lahondère, D., Lesimple, S., Maurizot, P., Paquette, J-L., Tarantola, A., Ulrich, M., 2020. Slab-derived origin of tremolite–antigorite veins in a supra-subduction ophiolite; the Peridotite Nappe (New Caledonia) as a case study. International Journal of Earth Science (Geologische Rundschau) 109, 171–196.

Collot, J., Geli, L., Lafoy, Y., Vially, R., Cluzel, D., Klingelhoefer, F., Nouzé, H., 2008. Tectonic history of northern New Caledonia Basin from deep offshore seismic reflection: Relation to late Eocene obduction in New Caledonia, southwest Pacific. Tectonics 27. https://doi.org/10.1029/2008TC002263

Collot, J., Patriat, M., Sutherland, R., Williams, S., Cluzel, D., Seton, M., Pelletier, B., Roest, W.R., Etienne, S., Bordenave, A., Maurizot, P., 2020. Geodynamics of the SW Pacific: a brief review and relations with New Caledonian geology. In: Maurizot, P., Mortimer, N. (Eds.), New Caledonia: Geology, Geodynamic Evolution and Mineral Resources. Geological Society, London, Memoirs, London 51, pp. 13-26.

Coney, P.J., 1980. Cordilleran metamorphic core complexes: An overview. In: Crittenden, M.D., Jr., Coney, P.J., Davis, G.H. (Eds.), Cordilleran Metamorphic Core Complexes. Geological Society of America, pp. 7-31.

Courjault, T., Grosheny, D., Ferry, S., Sausse, J., 2011. Detailed anatomy of a deep-water carbonate breccia lobe (Upper Jurassic, French subalpine basin). Sedimentary Geology 238, 156–171.

Crawford, A.J., Meffre, S., Symonds, P.A., 2003. 120 to 0 Ma tectonic evolution of the southwest Pacific and analogous geological evolution of the 600 to 220 Ma Tasman Fold Belt System. Geological Society of America Special Papers 372, 383–403.

Dallanave, E., Agnini, C., Bachtadse, V., Muttoni, G., Crampton, J.S., Strong, C.P., Hines, B.R., Hollis, C.J., Slotnick, B.S., 2015. Early to middle Eocene magneto-biochronology of the southwest Pacific Ocean and climate influence on sedimentation: Insights from the Mead Stream section, New Zealand. GSA Bulletin 127, 643–660.

Dallanave, E., Agnini, C., Pascher, K.M., Maurizot, P., Bachtadse, V., Hollis, C.J., Dickens, G.R., Collot, J., Monesi, E., 2018. Magneto-biostratigraphic constraints of the Eocene micrite–calciturbidite transition in New Caledonia: tectonic implications. New Zealand Journal of Geology and Geophysics 61, 145–163.

Dallanave, E., Maurizot, P., Agnini, C., Sutherland, R., Hollis, C.J., Collot, J., Dickens, G.R., Bachtadse, V., Strogen, D., Morgans, H.E.G., 2020. Eocene (46–44 Ma) onset of Australia-Pacific plate motion in the southwest Pacific inferred from stratigraphy in New Caledonia and New Zealand. Geochemistry, Geophysics, Geosystems 21, e2019GC008699. https://doi.org/10.1029/2019GC008699

Davis, G.A., Lister, G.S., Reynolds, S.J., 1986. Structural evolution of the Whipple and South mountains shear zones, southwestern United States. Geology 14, 7–10.

Davis, G.H., Coney, P.J., 1979. Geologic development of the Cordilleran metamorphic core complexes. Geology 7, 120–124.

Dewey, J. F., 1976. Ophiolite obduction. Tectonophysics 31, 93-120.

Driscoll, N.W., Hogg, J.R., Christie-Blick, N., Karner, G.D., 1995. Extensional tectonics in the Jeanne d'Arc Basin, offshore Newfoundland: implications for the timing of break-up between Grand Banks and Iberia. Geological Society, London, Special Publications 90, 1-28.

Dunham, R.J., 1962. Classification of carbonate rocks according to depositional textures. In: Ham, W.E. (Ed.), Classification of Carbonate Rocks--A Symposium, Memoir. AAPG Special Volumes, pp. 108–121.

Espirat, J.J., 1971. Carte et Notice Explicative de la Carte Géologique de la Nouvelle-Calédonie à l'Echelle du 1/50000: feuille Bourail. Bureau de Recherches Géologiques et Minières, Paris. (in French)

Etienne, S., Collot, J., Sutherland, R., Patriat, M., Bache, F., Rouillard, P., Henrys, S., Barker, D., Juan, C., 2018. Deepwater sedimentation and Cenozoic deformation in the Southern New Caledonia Trough (Northern Zealandia, SW Pacific). Marine and Petroleum Geology 92, 764–779.

Ferry, S., Grosheny, D., Backert, N., Atrops, F., 2015. The base-of-slope carbonate breccia system of Céüse (Tithonian, S-E France): Occurrence of progradational stratification in the head plug of coarse granular flow deposits. Sedimentary Geology 317, 71–86.

Festa, A., Ogata, K., Pini, G.A., Dilek, Y., Alonso, J.L., 2016. Origin and significance of olistostromes in the evolution of orogenic belts: A global synthesis. Gondwana Research 39, 180–203.

Flügel, E., 2013. Microfacies of Carbonate Rocks: Analysis, Interpretation and Application. Springer Science & Business Media. 975 pp.

Föllmi, K.B., 1996. The phosphorus cycle, phosphogenesis and marine phosphate-rich deposits. Earth-Science Reviews 40, 55–124.

France, R., 2000. PRA 436, New Caledonia: CADART-1 & CADART-1st Final Well Report. Victoria Petroleum, Nouvelle-Calédonie, Vol. 1, 66 pp.

Gaina, C., Müller, D.R., Royer, J.-Y., Stock, J., Hardebeck, J., Symonds, P., 1998. The tectonic history of the Tasman Sea: A puzzle with 13 pieces. Journal of Geophysical Research: Solid Earth 103, 12413–12433.

Galloway, W.E., 1998. Siliciclastic slope and base-of-slope depositional systems: Component facies, stratigraphic architecture, and classification. AAPG Bulletin 82, 569–595.

Gautier, P., Quesnel, B., Boulvais, P., Cathelineau, M., 2016. The emplacement of the Peridotite Nappe of New Caledonia and its bearing on the tectonics of obduction. Tectonics 35, 3070-3094.

Gonord, H., 1977. Recherches sur la Géologie de la Nouvelle-Calédonie, sa Place dans l'Ensemble Structural du Pacifique Sud-Ouest (Ph.D Thesis). Université de Montpellier, Montpellier, France. (in French)

Gradstein, F.M., Ogg, J.G., Smith, A.G., Ogg, G.M., 2012. The Geological Time Scale 2012. Elsevier, Boston, United State of America. 1144 pp.

Hancock, H.J.L., Dickens, G.R., Strong, C.P., Hollis, C.J., Field, B.D., 2003. Foraminiferal and carbon isotope stratigraphy through the Paleocene-Eocene transition at Dee Stream, Marlborough, New Zealand. New Zealand Journal of Geology and Geophysics 46, 1–19.

Hayes, D.E., Ringis, J., 1973. Seafloor spreading in the Tasman Sea. Nature 243, 454–458.

Hollis, C.J., 2007. Radiolarian faunal turnover through the Paleocene-Eocene transition, Mead Stream, New Zealand. In: Baumgartner, P.O., Aitchison, J.C., De Wever, P., Jackett, S.-J. (Eds.), Radiolaria. Birkhäuser Basel, Basel, pp. 79–99.

Hollis, C.J., Dickens, G.R., Field, B.D., Jones, C.M., Percy Strong, C., 2005. The Paleocene–Eocene transition at Mead Stream, New Zealand: a southern Pacific record of early Cenozoic global change. Palaeogeography, Palaeoclimatology, Palaeoecology 215, 313–343.

Hornibrook, N. de B., Brazier, R.C., Strong, C.P., 1989. Manual of New Zealand Permian to Pleistocene foraminiferal biostratigraphy. New Zealand Geological Survey Paleontological Bulletin 56, 175 pp.

Jenkins, D.G., 1971. New Zealand Cenozoic planktonic foraminifera. New Zealand Geological Survey Paleontological Bulletin 42, 278 pp.

Jolivet, L., Faccenna, C., Piromallo, C., 2009. From mantle to crust: Stretching the Mediterranean. Earth and Planetary Science Letters 285, 198–209.

Kastens, K.A., Shor, A.N., 1985. Depositional processes of a meandering channel on Mississippi Fan. AAPG Bulletin 69, 190–202.

Kerr, A.C., Tarney, J., Nivia, A., Marriner, G.F., Saunders, A.D., 1998. The internal structure of oceanic plateaus: inferences from obducted Cretaceous terranes in western Colombia and the Caribbean. Tectonophysics 292, 173–188.

Lagabrielle, Y., Cannat, M., 1990. Alpine Jurassic ophiolites resemble the modern central Atlantic basement. Geology 18, 319–322.

Lagabrielle, Y., Maurizot, P., Lafoy, Y., Cabioch, G., Pelletier, B., Régnier, M., Wabete, I., Calmant, S., 2005. Post-Eocene extensional tectonics in Southern New Caledonia (SW Pacific): Insights from onshore fault analysis and offshore seismic data. Tectonophysics 403, 1–28.

Lagabrielle, Y., Chauvet, A., Ulrich, M., Guillot, S., 2013. Passive obduction and gravity-driven emplacement of large ophiolitic sheets: The New Caledonia ophiolite (SW Pacific) as a case study? Bulletin de la Société Géologique de France 184, 545-556.

Le Pichon, X., Angelier, J., Osmaston, M.F., Stegena, L., Vine, F.J., Smith, A.G., 1981. The Aegean Sea. Philosophical Transactions of the Royal Society of London. Series A, Mathematical and Physical Sciences 300, 357–372.

Liu, Q., Kneller, B., Fallgatter, C., Valdez Buso, V., Milana, J.P., 2018. Tabularity of individual turbidite beds controlled by flow efficiency and degree of confinement. Sedimentology 65, 2368–2387.

Manatschal, G., Müntener, O., 2009. A type sequence across an ancient magma-poor ocean–continent transition: the example of the western Alpine Tethys ophiolites. Tectonophysics 473, 4–19.

Martini, E., 1971. Standard Tertiary and Quaternary calcareous nannoplankton zonation. In: Farinacci, A. (Ed.), Proceedings of the Second Planktonic Conference, Roma, Italy, pp. 739–785.

Mason, P., Huntington, J.F., 2012. HyLogger 3 components and pre-processing: An overview. Northern Territory Geological Survey, Darwin, Australia, Technical Note 2012-02, 9 pp.

Maurizot, P., 2011. First sedimentary record of the pre-obduction convergence in New Caledonia: formation of an Early Eocene accretionary complex in the north of Grande Terre and emplacement of the 'Montagnes Blanches' nappe. Bulletin de la Société Géologique de France 182, 479–491.

Maurizot, P., 2012. Palaeocene age for the Adio Limestone, New Caledonia: stratigraphic and regional context. New Zealand Journal of Geology and Geophysics 56, 16–26.

Maurizot, P., 2014. Evolution and sedimentation in a forebulge environment: example of the late Eocene Uitoé Limestone, New Caledonia, Southwest Pacific. New Zealand Journal of Geology and Geophysics 57, 390–401.

Maurizot, P., Vendé-Leclerc, M., 2009. Carte Géologique de la Nouvelle-Calédonie au 1/ 500 000, Notice explicative par Maurizot, P., Collot, J., 2009. Direction de l'Industrie, des Mines et de l'Energie de Nouvelle-Calédonie, Bureau de Recherches Géologiques et Minières, Nouméa. (in French)

Maurizot, P., Cluzel, D., 2014. Pre-obduction records of Eocene foreland basins in central New Caledonia: an appraisal from surface geology and Cadart-1 borehole data. New Zealand Journal of Geology and Geophysics 57, 300–311.

Maurizot, P., Cabioch, G., Fournier, F., Leonide, P., Sebih, S., Rouillard, P., Montaggioni, L., Collot, J., Martin-Garin, B., Chaproniere, G., 2016. Post-obduction carbonate system development in New Caledonia (Népoui, Lower Miocene). Sedimentary Geology 331, 42–62.

Maurizot, P., Bordenave, A., Cluzel, D., Collot, J., Etienne, S., 2020a. Late Cretaceous to Eocene cover of New Caledonia: from rifting to convergence. In: Maurizot, P., Mortimer, N. (Eds.), New Caledonia: Geology, Geodynamic Evolution and Mineral Resources. Geological Society, London, Memoirs, London 51, pp. 53-91

Maurizot, P., Cluzel, D., Patriat, M., Collot, J., Iseppi, M., Lesimple, S., Secchiari, A., Bosch, D., Montanini, A., Macera, P., Davies, H.L., 2020b. The Eocene Subduction–Obduction Complex of New Caledonia. In: Maurizot, P., Mortimer, N. (Eds.), New Caledonia: Geology, Geodynamic Evolution and Mineral Resources. Geological Society, London, Memoirs, London 51, pp. 93-130.

McAlpine, K.D., 1990. Mesozoic Stratigraphy, Sedimentary Evolution, and Petroleum Potential of the Jeanne D'Arc Basin, Grand Banks of New Foundland. Geological Survey of Canada Ottawa, Canada, Vol. 89, No. 17, 56 pp.

Meffre, S., 1991. Terrane Analysis of New Caledonia with Special Reference to the Koh Area. (B.Sc. Honours thesis), University of Sydney, Sydney, Australia.

Meffre, S., Aitchison, J.C., Crawford, A.J., 1996. Geochemical evolution and tectonic significance of boninites and tholeiites from the Koh ophiolite, New Caledonia. Tectonics 15, 67–83.

Miller, K.G., Kominz, M.A., Browning, J.V., Wright, J.D., Mountain, G.S., Katz, M.E., Sugarman, P.J., Cramer, B.S., Christie-Blick, N., Pekar, S.F., 2005. The Phanerozoic record of global sea-level change. Science 310, 1293-1298.

Mortimer, N., Herzer, R.H., Walker, N.W., Calvert, A.T., Seward, D., Chaproniere, G.C., 2003. Cavalli Seamount, Northland Plateau, SW Pacific Ocean: a Miocene metamorphic core complex? Journal of the Geological Society 160, 971-983.

Mortimer, N., Herzer, R.H., Gans, P.B., Laporte-Magoni, C., Calvert, A.T., Bosch, D., 2007. Oligocene–Miocene tectonic evolution of the South Fiji Basin and Northland Plateau, SW Pacific Ocean: Evidence from petrology and dating of dredged rocks. Marine Geology 237, 1–24.

Mortimer, N., Raine, J.I., Cook, R.A., 2009. Correlation of basement rocks from Waka Nui-1 and Awhitu-1, and the Jurassic regional geology of Zealandia. New Zealand Journal of Geology and Geophysics 52, 1–10.

Mortimer, N., Campbell, H.J., Tulloch, A.J., King, P.R., Stagpoole, V.M., Wood, R.A., Rattenbury, M.S., Sutherland, R., Adams, C.J., Collot, J., Seton, M., 2017. Zealandia: Earth's hidden continent. GSA Today. https://doi.org/10.1130/GSATG321A.1

Mortimer, N., Patriat, M., Gans, P.B., Agranier, A., Chazot, G., Collot, J., Crundwell, M.P., Durance, P.M.J., Campbell H.J., Etienne, S., 2020. The Norfolk Ridge seamounts: Eocene–Miocene volcanoes near Zealandia's rifted continental margin. Australian Journal of Earth Sciences, https://doi.org/10.1080/08120099.2020.1805007

Mulder, T., Alexander, J., 2001. The physical character of subaqueous sedimentary density flows and their deposits. Sedimentology 48, 269–299.

Mulder, T., Etienne, S., 2010. Lobes in deep-sea turbidite systems: State of the art. Sedimentary Geology 229, 75–80.

Mutti, E., 1992. Turbidite sandstones. Agip, Istituto di geologia, Università di Parma. 275 pp.

Mutti, E., Sonnino, M., 1981. Compensation cycles: a diagnostic feature of turbidite sandstone lobes. International Association of Sedimentologists, 2nd European Regional Meeting, Abstract, Bologna, Italy, pp. 120-123.

Nicholson, K.N., Maurizot, P., Black, P.M., Picard, C., Simonetti, A., Stewart, A., Alexander, A., 2011. Geochemistry and age of the Nouméa Basin lavas, New Caledonia: Evidence for Cretaceous subduction beneath the eastern Gondwana margin. Lithos 125, 659–674.

O'Connor, J.M., Steinberger, B., Regelous, M., Koppers, A.A.P., Wijbrans, J.R., Haase, K.M., Stoffers, P., Jokat, W., Garbe-Schönberg, D., 2013. Constraints on past plate and mantle motion from new ages for the Hawaiian-Emperor Seamount Chain. Geochemistry, Geophysics, Geosystems 14, 4564–4584.

Olsson, R.K., Berggren, W.A., Hemleben, C., Smewing, J.D., 1999. Atlas of Paleocene Planktonic Foraminifera. Smithsonian Contribution to Paleobiology. Smithsonian Institution Press, Washington D.C 85, 225 pp.

Paquette, J., Cluzel, D., 2006. U–Pb zircon dating of post-obduction volcanic-arc granitoids and a granulite-facies xenolith from New Caledonia. Inference on Southwest Pacific geodynamic models. International Journal of Earth Sciences 96**,** 613–622.

Paris, J.-P., 1981. Géologie de la Nouvelle-Calédonie : un Essai de Synthèse. Mémoire du Bureau de Recherche Géologique et Minière 113, 279 pp. (in French)

Pearson, P.N., Olsson, R.K., Huber, B.T., Hemleben, C., Berggren, W.A., 2006. Atlas of Eocene Planktonic Foraminifera. Cushman Foundation Special Publication 41, Fredericksburg, USA, 514 pp.

Pelletier, B., Calmant, S., Pillet, R., 1998. Current tectonics of the Tonga–New Hebrides region. Earth and Planetary Science Letters 164, 263–276.

Perch Nielsen, K., 1985. Cenozoic calcareous nannofossils. In: Bolli, H.M., Saunders, J.B., Perch-Nielsen, K. (Eds.), Plankton Stratigraphy. Cambridge, United Kingdom, pp. 427–554.

Pickering, K.T., Hiscott, R.N., Hein, F.J., 1989. Deep Marine Environments: Clastic Sedimentation and Tectonics. Unwin Hyman, London, 416 pp

Pomeyrol, R., 1955. Synthèse des Résultats Obtenus à la Date du 30 Avril 1955. Rapport S.R.E.P.N.C. Société de Recherche et d'Exploitation de Pétrole en Nouvelle Calédonie,

Richards, M., Bowman, M., Reading, H., 1998. Submarine-fan systems I: characterization and stratigraphic prediction. Marine and Petroleum Geology 15, 689–717.

Robaszynski, F.,Caron, M., Gonzalez Donoso, J.M., Wonders, A.A.H., 1994. Atlas of Late Cretaceous Globotruncanids. Revue de Micropaleontologie 26, 145-305

Routhier, P., 1953. Etude Géologique du Versant Occidental de la Nouvelle Calédonie entre le Col de Boghen et la Pointe d'Arama. Mémoire de la Société Géologique de France 32, 271 pp. (in French)

Schellart, W.P., Lister, G.S., Toy, V.G., 2006. A Late Cretaceous and Cenozoic reconstruction of the Southwest Pacific region: Tectonics controlled by subduction and slab rollback processes. Earth Science Reviews 76, 191–233.

Sdrolias, M., Müller, R.D., Gaina, C., 2003. Tectonic evolution of the southwest Pacific using constraints from backarc basins. Geological Society of America Special Papers 372, 343–359.

Secchiari, A., Becker, H., Gleißner, P., Li, C., Montanini, A., Bosch, D. 2017. Evidence from the New Caledonia peridotites for contrasting behavior of highly siderophile and chalcophile elements in supra-subduction zone and normal upper mantle. Congresso, Società Italianan di Mineralogia e Petrografia, Socieità Geologica Italiana, Associazone Italian di Vulcanologia; Società Geochimica Italiana (SIMPSGI-SOGEI-AIV), 4–6 September 2017, Pisa, Italy, pp. 285.

Slotnick, B., Dickens, G., Hollis, C., Crampton, J., Percy Strong, C., Phillips, A., 2015. The onset of the Early Eocene Climatic Optimum at Branch Stream, Clarence River valley, New Zealand. New Zealand Journal of Geology and Geophysics 58, 262–280.

Smith, W.H.F., Sandwell, D.T., 1997. Global sea floor topography from satellite altimetry and ship depth soundings. Science 277, 1956–1962.

Stow, D.A.V., 2005. Sedimentary Rocks in the Field: a Colour Guide. Manson Publishing, London, 320 pp.

Stow, D.A.V., Howell, D.G., Nelson, C.H., 1984. Sedimentary, tectonic, and sea-level controls on submarine fan and slope-apron turbidite systems. Geo-Marine Letters 3, 57–64.

Sutherland, R., Collot, J., Lafoy, Y., Logan, G.A., Hackney, R., Stagpoole, V., Uruski, C., Hashimoto, T., Higgins, K., Herzer, R.H., Wood, R., Mortimer, N., Rollet, N., 2010. Lithosphere delamination with foundering of lower crust and mantle caused permanent subsidence of New Caledonia Trough and transient uplift of Lord Howe Rise during Eocene and Oligocene initiation of Tonga-Kermadec subduction, western Pacific. Tectonics 29, TC2004. https://doi.org/10.1029/2009TC002476

Sutherland, R., Collot, J., Bache, F., Henrys, S., Barker, D., Browne, G.H., Lawrence, M.J.F., Morgans, H.E.G., Hollis, C.J., Clowes, C., Mortimer, N., Rouillard, P., Gurnis, M., Etienne, S., Stratford, W., 2017. Widespread compression associated with Eocene Tonga-Kermadec subduction initiation. Geology 45, 355–358.

Sutherland, R., Dickens, G.R., Blum, P., Alegret, L., Asatryan, G., Bhattacharya, J., Bordenave, A., Chang, L., Collot, J., Cramwinckel, M.J., Dallanave, E., Drake, M.K., Etienne, S.J.G., Giorgioni, M., Gurnis, M., Harper, D.T., Huang, H.-H.M., Keller, A.L., Lam, A.R., Matsui, H., Morgans, H.E.G., Newsam, C., Park, Y.-H., Pascher, K.M., Pekar, S.F., Penman, D.E., Saito, S., Stratford, W.R., Westerhold, T., Zhou, X., 2018. Expedition 371 Preliminary Report: Tasman Frontier Subduction Initiation and Paleogene Climate. International Ocean Discovery Program, Tasman Frontier Subduction Initiation and Paleogene Climate 371. https://doi.org/10.14379/iodp.pr.371.2018

Sutherland, R., Dickens, G.R., Blum, P., Alegret, L., Asatryan, G., Bhattacharya, J., Bordenave, A., Chang, L., Collot, J., Cramwinckel, M.J., Dallanave, E., Drake, M.K., Etienne, S.J.G., Giorgioni, M., Gurnis, M., Harper, D.T., Huang, H.-H.M., Keller, A.L., Lam, A.R., Matsui, H., Morgans, H.E.G., Newsam, C., Park, Y.-H., Pascher, K.M., Pekar, S.F., Penman, D.E., Saito, S., Stratford, W.R., Westerhold, T., Zhou, X., 2019. Site U1507. In Sutherland, R., Dickens, G.R., Blum, P., the Expedition 371 Scientists (Eds.), Tasman Frontier Subduction Initiation and Paleogene Climate. Proceedings of the International Ocean Discovery Program, 371: College Station, Texas, USA, (International Ocean Discovery Program). https://doi.org/10.14379/iodp.proc.371.104.2019

Sutherland, R., Dickens, G.R., Blum, P., Agnini, C., Alegret, L., Asatryan, G., Bhattacharya, J., Bordenave, A., Chang, L., Collot, J., Cramwinckel, M.J., Dallanave, E., Drake, M.K., Etienne, S.J.G., Giorgioni, M., Gurnis, M., Harper, D.T., Huang, H.-H.M., Keller, A.L., Lam, A.R., Li, H., Matsui, H., Morgans, H.E.G., Newsam, C., Park, Y.-H., Pascher, K.M., Pekar, S.F., Penman, D.E., Saito, S., Stratford, W.R., Westerhold, T., Zhou, X., 2020. Continental-scale geographic change across Zealandia during Paleogene subduction initiation. Geology 48. https://doi.org/10.1130/G47008.1

Tirel, C., Brun, J.-P., Burov, E., 2004. Thermo-mechanical modeling of extensional gneiss dome. In: Whitney, D.L., Teyssier, C., Siddoway, C.S. (Eds.), Gneiss Domes and Orogeny. Geological Society of America Bulletin 380. https://doi.org/10.1130/0-8137-2380-9.67

Tirel, C., Brun, J.-P., Burov, E., 2008. Dynamics and structural development of metamorphic core complexes. Journal of Geophysical Research: Solid Earth 113. https://doi.org/10.1029/2005JB003694

Tissot, B., Noesmoen, A., 1958. Les bassins de Nouméa et de Bourail (Nouvelle-Calédonie). Revue de l’Institut Français du Pétrole 13, 739–759. (in French)

Tokuyama, H., Kuramoto, S.I., Soh, W., Miyashita, S., Byrne, T., Tanaka, T., 1992. Initiation of ophiolite emplacement: a modern example from Okushiri Ridge, Northeast Japan Arc. Marine Geology 103, 323-334.

Tournadour, E., Fournier, F., Etienne, S., Collot, J., Maurizot, P., Patriat, M., Sevin, B., Morgans, H.E.G., Martin-Garin, B., Braga, J.C., 2020. Seagrass-related carbonate ramp development at the front of a fan delta (Burdigalian, New Caledonia): Insights into mixed carbonate-siliciclastic environments. Marine and Petroleum Geology 121, 104581. https://doi.org/10.1016/j.marpetgeo.2020.104581

Vitale Brovarone, A., Agard, P., Monié, P., Chauvet, A., Rabaute, A., 2018. Tectonic and metamorphic architecture of the HP belt of New Caledonia. Earth-Science Reviews 178, 48–67.

Weber, M.E., Reilly, B.T., 2018. Hemipelagic and turbiditic deposits constrain lower Bengal Fan depositional history through Pleistocene climate, monsoon, and sea level transitions. Quaternary Science Reviews 199, 159–173.

Weissel, J.K., Hayes, D.E., 1977. Evolution of the Tasman Sea reappraised. Earth and Planetary Science Letters 36, 77–84.

Wernicke, B., 1981. Low-angle normal faults in the Basin and Range Province: nappe tectonics in an extending orogen. Nature 291, 645–648.

Wernicke, B., 1985. Uniform-sense normal simple shear of the continental lithosphere. Canadian Journal of Earth Sciences 22, 108–125.

Wernicke, B., Burchfiel, B.C., 1982. Modes of extensional tectonics. Journal of Structural Geology 4, 105–115.

Whattam, S.A., Malpas, J., Ali, J.R., Smith, I.E.M., 2008. New SW Pacific tectonic model: Cyclical intraoceanic magmatic arc construction and near-coeval emplacement along the

Australia-Pacific margin in the Cenozoic. Geochemistry, Geophysics, Geosystems 9. https://doi.org/10.1029/2007gc001710

Wuellner, D.E., James, W.C., 1989. Braided and meandering submarine fan channel deposits, Tesnus Formation, Marathon Basin, West Texas. Sedimentary Geology 62, 27–45.

Zachos, J., Pagani, M., Sloan, L., Thomas, E., Billups, K., 2001. Trends, rhythms, and aberrations in global climate 65 Ma to Present. Science 292, 686.

Zachos, J.C., Dickens, G.R., Zeebe, R.E., 2008. An early Cenozoic perspective on greenhouse warming and carbon-cycle dynamics. Nature 451, 279–283.

Figure captions

Figure. 1: **(a)** Regional bathymetric map of the south west Pacific between New Caledonia (NC), New Zealand (NZ) and Australia (AU) with location of the main morphobathymetric features. Red dotted line delimitates the Zealandia continent (Mortimer et al., 2017). Bathymetric data are from Global Predicted Bathymetry V18.1 (Smith and Sandwell, 1997). **(b)** Simplified geological map of New Caledonia modified after (Maurizot and Vendé-Leclerc, 2009). The black rectangle shows the location of the study area. **(c)** Simplified geological cross section of Grande Terre modified after Maurizot and Vendé-Leclerc (2009).

Figure. 2: Lithostratigraphy of the New Caledonian sedimentary succession from Upper Cretaceous to Oligocene (modified after Tissot and Noesmoen, 1958; Avias, 1967; Paris, 1981; Cluzel et al., 2001, 2018; Maurizot, 2011; Maurizot and Cluzel, 2014; Maurizot et al., 2020a). Lithostratigraphic units are associated with the major tectonic events which marked New Caledonian geological history. St= silt; F= fine; M= medium; Pbl; pebble.

Figure. 3: **(a)** Geological map of the Bourail anticline and position of the CADART-1 well complemented with the Nera River section (after Maurizot et al., 2020a). **(b)** Schematic cross section of the Bourail anticline showing the CADART-1 / Nera River section.

Figure. 4: Composite log of the CADART-1 well and Nera River section with new lithostratigraphic divisions and subdivisions from this study. Relative thicknesses are from bottom and top of the CADART-1 well. Samples for petrography, biostratigraphy and mineralogical point counting analysis are shown.

Figure. 5: **(a)** Core photo of the six main facies associations present in the Gouaro Formation and in the Mamelons Rouges Beds Formation. **(b)** Core photo of secondary pyritic mineralization and **(c)** Dendritic white gypsum mineralisation on core surfaces observed along the “Mamelons Rouges Beds Formation”.

Figure. 6: **(a)** Synthetic sedimentological log (1:500 scale description) of the Gouaro Formation illustrating lithofacies succession. The legend of facies association is detailed in Fig. 4. **(b)** Graphic sedimentary log (1:50 scale description) illustrating the facies succession in a sandy package. Hyperspectral data are shown in SWIR (short-wave infrared region) and TIR (thermal infrared region) wavelength domain. Cl= clay; St= silt; vF= very fine; F= fine; M= medium; C= coarse; vC= very coarse; G= granule; Pbl= pebbles; Cbl= cobbles.

Figure. 7: **(a)** Well core photos of the four facies associations present in the Adio Limestone Formation. **(b)** Well core photo zoomed on particular features of this formation: **1**. Soft sediment deformation; **2**. burrow filled by bioclastic grainstone; **3**. Sharp grain size increase in middle of FAc1; **4**. Erosional basal contact of bioclastic grainstone bed.

Figure. 8: Synthetic sedimentological log (1:500 scale description) of the Adio Limestone Formation illustrating lithofacies succession and mineralogical composition from hyperspectral data in the SWIR (short-wave infrared region) and TIR (thermal infrared region) wavelength domains. v.F= very fine; F= fine; M= medium; C= coarse; v.C= very coarse; G= granule.

Figure. 9: (a) Well core photos of the five main facies associations present in the Lower Bourail Flysch Formation. These facies associations are described in Table 1.

Figure. 10: (a) Synthetic sedimentological log (1:500 scale description) of the Lower Bourail Flysch Formation illustrating facies association successions in one of the sandy packages. See Fig. 4 for the facies association legend. **(b)** Graphic sedimentary log (1:50 scale description) illustrating facies succession in a sandy-dominated interval. Hyperspectral data are shown in SWIR (short-wave infrared region) and TIR (thermal infrared region) wavelength domain. Cl= clay; St= silt; v.F= very fine; F= fine; M= medium; C= coarse; v.C= very coarse; G= granule; Pbl= pebbles; Cbl= cobbles.

Figure. 11: (a) Typical coarsening and thickening upward metric sequence of calcareous sandstone present in the Middle Bourail Flysch Formation. See Fig. 4 for the facies association legend. **(b)** Photo of 2 mains facies association present in this formation. Cl= clay; St= silt; v.F= very fine; F= fine.

Figure. 12: Main features of the Upper Bourail Flysch Formation. **(a)** Centimetre-thick turbiditic bed of normal-graded, medium grained clinopyroxene rich sandstone interbedded with argillites. **(b)** Metre-thick turbiditic bed of coarse grained clinopyroxene rich sandstone with traction carpet marked by centimetre-thick sedimentary clasts. **(c)** Polygenic, clast supported, moderately sorted, subangular clasts breccia with a clinopyroxene rich sandstone matrix. **(d)** Polygenic, matrix supported, subangular and moderately sorted breccia with micritic mudstone, silicified mudrock and sandstone clasts. **(e)** Poorly sorted, polygenic, matrix supported breccia with clinopyroxene rich sandstone matrix. Silicified mudrocks, micritic mudstones with planktonic foraminifera and siliceous nodules, sandstone and siltstone clasts, and foraminifera-rich, shell debris-rich bioclastic grainstone with red algae and coral fragments are the main components of these breccias.

Figure. 13: Outcrop photos of different breccia facies present in the Upper Bourail Flysch Formation. **(a)** Outcrops panorama of the Upper Bourail Flysch member with typical clinopyroxene rich lithofacies FAm4/FAm5 and slumped surfaces (red lines). **(b)** Interbedded clinopyroxene rich sandstone (yellow colour) with thick bedded, erosional base (red line), moderately sorted, angular and polygenic clasts breccia (purple colour) with mega-ripples (dotted black line) which show a westward palaeocurrent direction.

Figure 14: Examples of micro-facies observed on thin sections from samples collected along the CADART-1 / Nera River section for each lithostratigraphic formations. Stratigraphic position of each sample is indicated in Fig. 4. **(a)** Micro-facies of the Gouaro Formation and the Mamelons Rouges Beds Formation. **1:** Moderately sorted, fine-grained sandstone with

subangular quartz, feldspar, and biogenic debris (Inoceram?) (FAm3). **2:** Well sorted, siltstone with subangular quartz and feldspar minerals and muddy matrix (FAm6). **3.** Well sorted, very-fine grained sandstone with angular quartz and feldspar (FAm5). **(b)** Micro-facies observed on the Adio Limestone Formation. **4:** Bioclastic grainstone with shell and bryozoan debris and siliciclastic clast as subrounded quartz grain (FAc1); **5**: Micritic mudstone with planktonic foraminifers (FAc4). **(c)** Micro-facies of the Lower Bourail Flysch Formation. **6:** Poorly sorted, fine-grained sandstone with subangular quartz, sedimentary lithics and undifferentiated biogenic debris (FAm3). **7:** Well sorted, fine-grained sandstone with subangular quartz, feldspar and silicified mudrock clast (FAm4). (**d**) Micro-facies of the Middle Bourail Flysch Formation. **8:** Poorly sorted, medium-grained calcareous sandstone with benthic foraminifers, algae clasts and quartz grains (FAm4). **9:** Poorly sorted, medium to fine-grained calcareous sandstone with benthic foraminifers debris, angular to subangular quartz and feldspar grains and coarse grain size of sedimentary lithics (FAm4). **10:** Moderately to well sorted siliciclastic limestone with a grainstone texture and millimetre thick benthic foraminifers (numulites) (FAm4). **(e)** Micro-facies of the Upper Bourail Flysch Formation. **11:** Moderately sorted, medium-grained sandstone with angular quartz and feldspar grains and subrounded sedimentary lithics as silicified mudrock clasts and siltstone clasts (FAm2). **12:** Well sorted, medium-grained clinopyroxene-rich sandstone with medium grain size silicified mudrock clasts (FAm3). **13:** Well sorted, fine-grained cpx-rich sandstone with presence of subrounded quartz, silicified mudrock clasts and micritic mudstone clasts (FAm3).

Figure. 15: Evolution of depositional change and interpretation of sedimentary processes, sources and vertical evolution of series present along the CADART-1 / Nera River section.

Table captions

Table. 1: Table summarising lithofacies and equivalence with Mutti facies (Mutti, 1992) and interpretations in terms of flow processes based on Mulder and Alexander (2001). Cl= clay; vF= very fine; M= medium; vC= very coarse; Pbl= pebbles.

Appendix

Appendix A: Mineralogical point-counting result along the Bourail Flysch Group in the CADART-1 well and Nera Rive section. Planktonic and Benthic foraminifera, Siliciclastic, Calcareous, Chert, Metamorphic / Volcanic clast, Clinopyroxene, Feldspar and Quartz are the main component of the Bourail Flysch Group. See Figure 4 for composite and Hyperspectral legend.

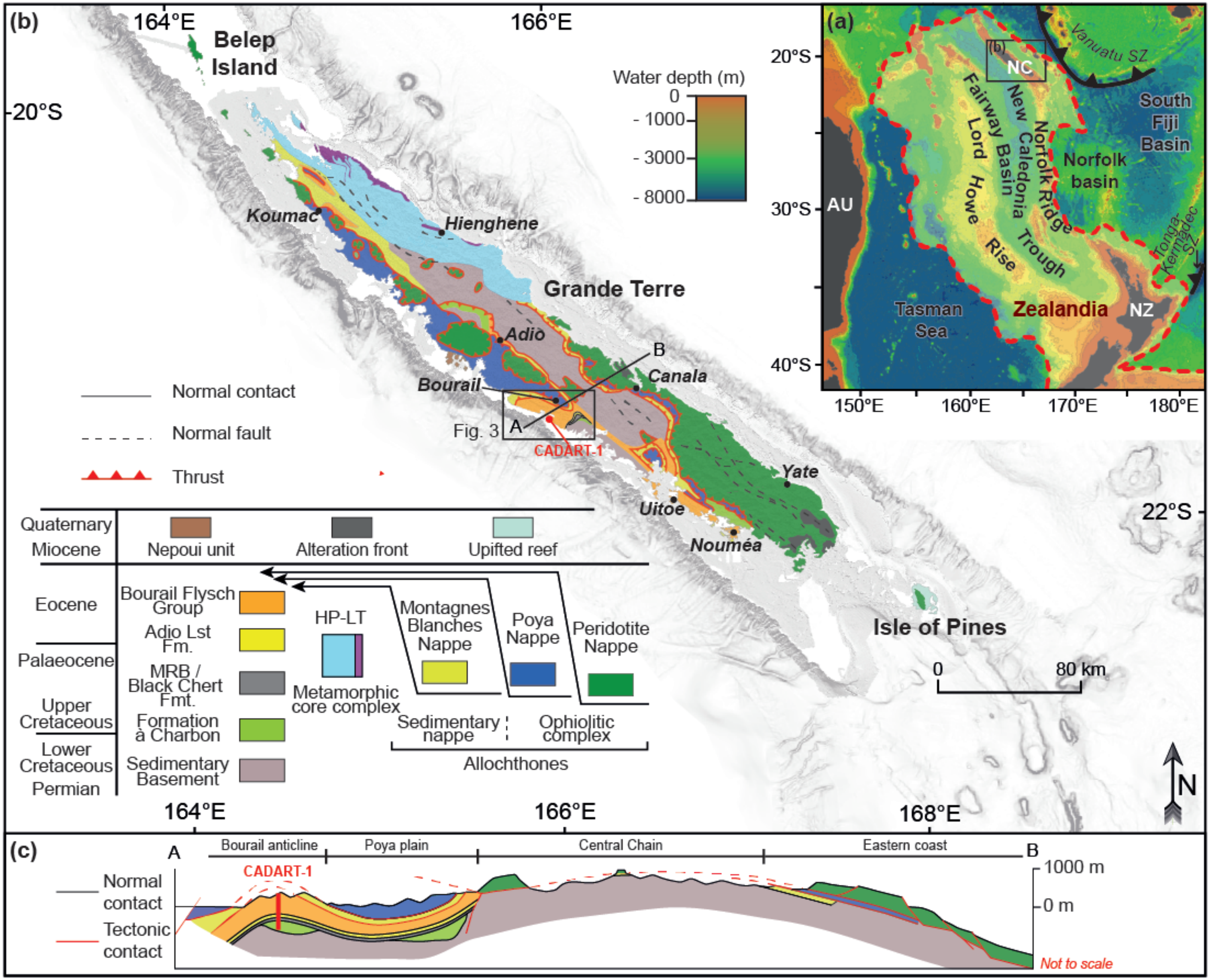

(b)
164°E
166°E
Belep Island
-20°S
Water depth (m)
0
- 1000
- 3000
- 8000
Koumac
Hienghene
Grande Terre
Adio
B
Canala
Bourail
Fig. 3
A
CADART-1
Normal contact
Normal fault
Thrust
Yate
Uitoe
Nouméa
22°S
Quaternary
Miocene
Nepoui unit
Alteration front
Upifted reef
Eocene
Bourail Flysch Group
Adio Lst Fm.
Palaeocene
MRB / Black Chert Fmt.
Upper Cretaceous
Formation à Charbon
Lower Cretaceous
Permian
Sedimentary Basement
HP-LT
Metamorphic core complex
Montagnes Blanches Nappe
Poya Nappe
Peridotite Nappe
Sedimentary nappe
Ophiolitic complex
Allochthones
Isle of Pines
0
80 km
N
164°E
166°E
168°E
(a)
20°S
30°S
40°S
(b)
NC
Vanuatu SZ
South Fiji Basin
Norfolk basin
Fairway Basin
New Caledonia Trough
Norfolk Ridge
Lord Howe Rise
AU
Tonga-Kermadec SZ
Tasman Sea
Zealandia
NZ
150°E
160°E
170°E
180°E
(c)
A
Bourail anticline
Poya plain
Central Chain
Eastern coast
B
CADART-1
1000 m
0 m
Normal contact
Tectonic contact
Not to scale

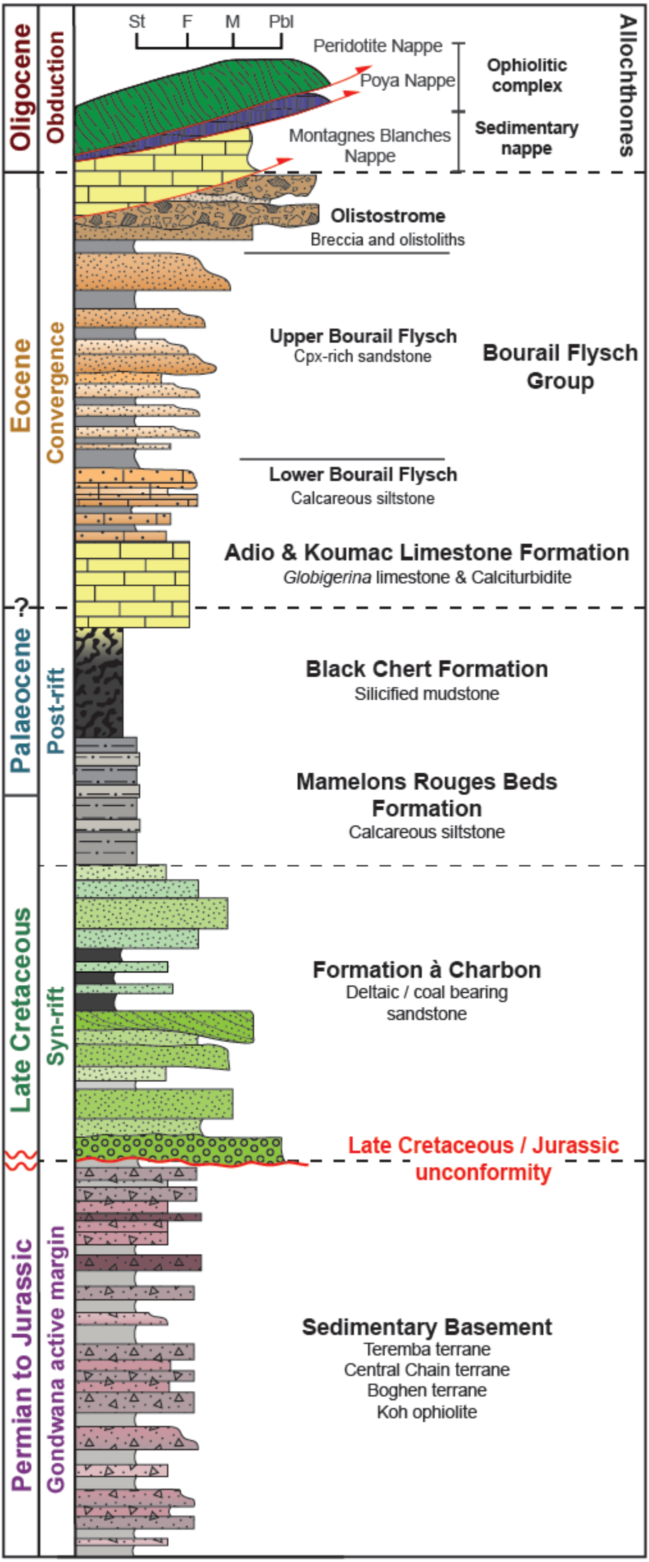
St
F
M
Pbl
Peridotite Nappe
Poya Nappe
Montagnes Blanches Nappe
Ophiolitic complex
Sedimentary nappe
Allochthones
Oligocene
Obduction
Olistostrome
Breccia and olistoliths
Upper Bourail Flysch
Cpx-rich sandstone
Bourail Flysch Group
Lower Bourail Flysch
Calcareous siltstone
Adio & Koumac Limestone Formation
Globigerina limestone & Calciturbidite
Eocene
Convergence
?
Black Chert Formation
Silicified mudstone
Mamelons Rouges Beds Formation
Calcareous siltstone
Palaeocene
Post-rift
Formation à Charbon
Deltaic / coal bearing sandstone
Late Cretaceous
Syn-rift
Late Cretaceous / Jurassic unconformity
Sedimentary Basement
Teremba terrane
Central Chain terrane
Boghen terrane
Koh ophiolite
Permian to Jurassic
Gondwana active margin

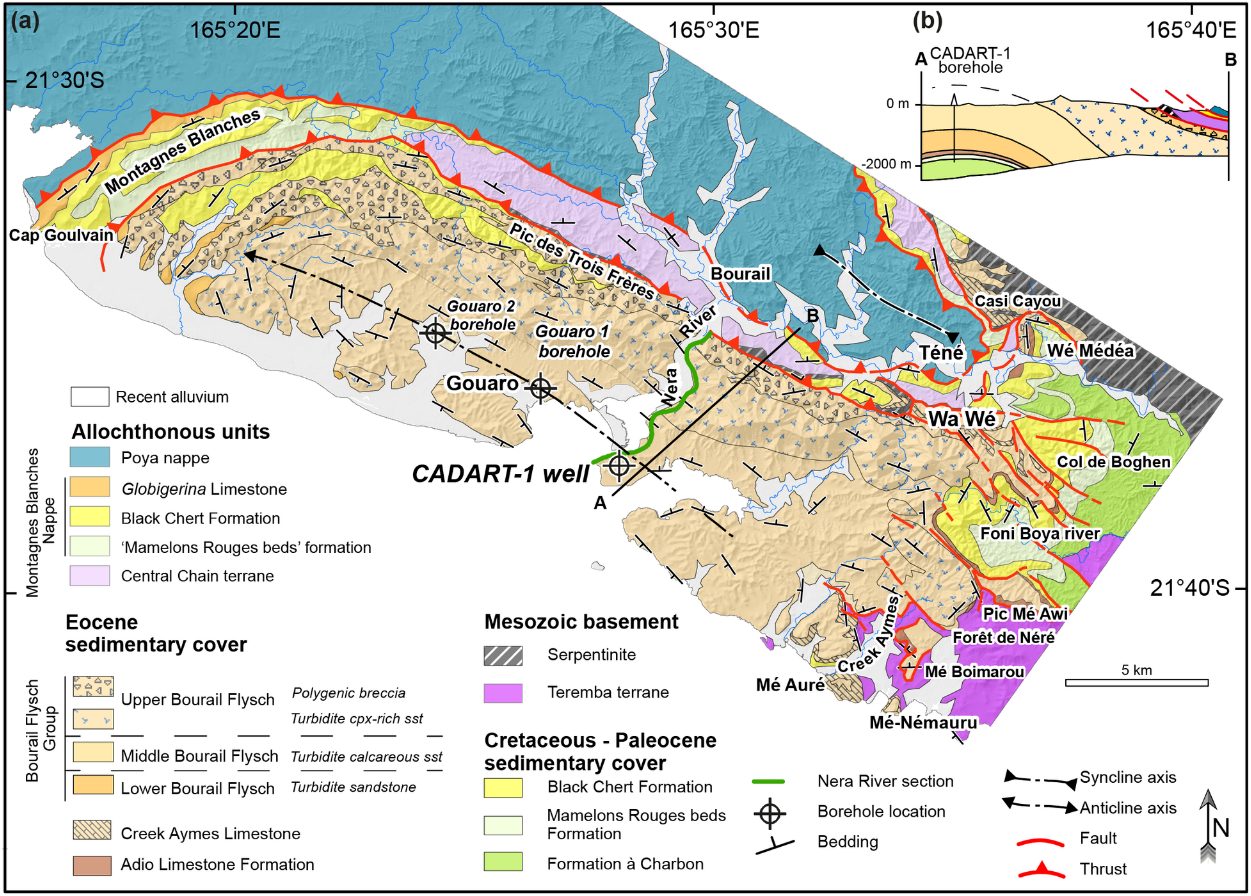

(a)
165°20'E
165°30'E
(b)
165°40'E
21°30'S
21°40'S
A
CADART-1
borehole
B
0 m
-2000 m
Montagnes Blanches
Cap Goulvain
Pic des Trois Frères
Bourail
Gouaro 2
borehole
Gouaro 1
borehole
Nera
River
Gouaro
CADART-1 well
A
B
Casi Cayou
Téné
Wé Médéa
Wa Wé
Col de Boghen
Foni Boya river
Pic Mé Awi
Forêt de Néré
Mé Boimarou
Creek Aymes
Mé Auré
Mé-Némauru
5 km
Recent alluvium
Allochthonous units
Poya nappe
Montagnes Blanches Nappe
Globigerina Limestone
Black Chert Formation
'Mamelons Rouges beds' formation
Central Chain terrane
Eocene
sedimentary cover
Bourail Flysch Group
Upper Bourail Flysch
Polygenic breccia
Turbidite cpx-rich sst
Middle Bourail Flysch
Turbidite calcareous sst
Lower Bourail Flysch
Turbidite sandstone
Creek Aymes Limestone
Adio Limestone Formation
Mesozoic basement
Serpentinite
Teremba terrane
Cretaceous - Paleocene
sedimentary cover
Black Chert Formation
Mamelons Rouges beds
Formation
Formation à Charbon
Nera River section
Borehole location
Bedding
Syncline axis
Anticline axis
Fault
Thrust
N

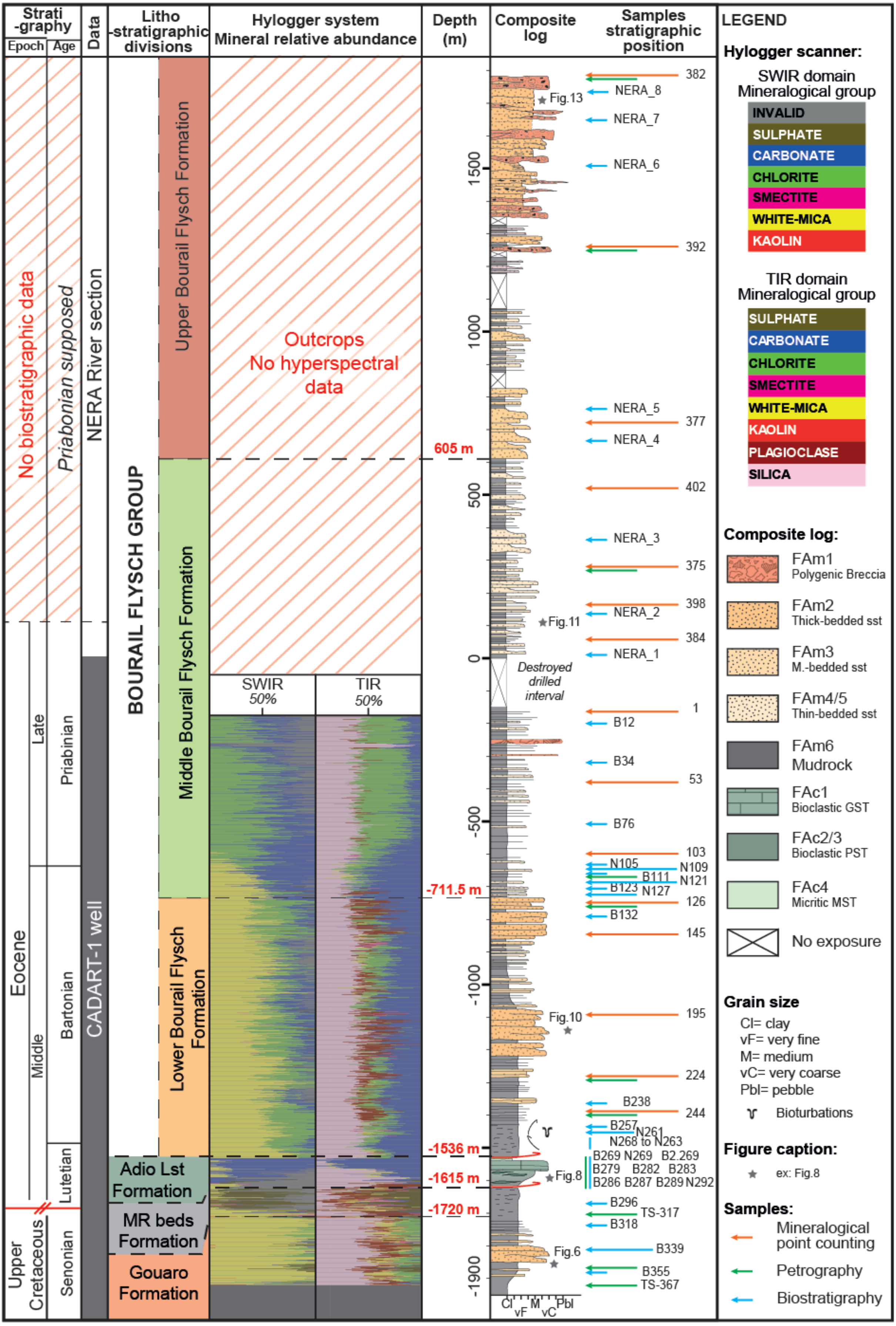

Strati-graphy
Epoch
Age
Data
Litho-stratigraphic divisions
Hylogger system Mineral relative abundance
Depth (m)
Composite log
Samples stratigraphic position
LEGEND
No biostratigraphic data
Priabonian supposed
NERA River section
Upper Bourail Flysch Formation
Outcrops
No hyperspectral data
605 m
BOURAIL FLYSCH GROUP
Middle Bourail Flysch Formation
SWIR 50%
TIR 50%
Eocene
Late
Middle
Priabonian
Bartonian
Lutetian
Upper Cretaceous
Senonian
CADART-1 well
Lower Bourail Flysch Formation
Adio Lst Formation
MR beds Formation
Gouaro Formation
-711.5 m
-1536 m
-1615 m
-1720 m
1500
1000
500
0
-500
-1000
-1900
Destroyed drilled interval
Cl vF M vC Pbl
Fig.13
Fig.11
Fig.10
Fig.8
Fig.6
382
NERA_8
NERA_7
NERA_6
392
NERA_5
377
NERA_4
402
NERA_3
375
398
NERA_2
384
NERA_1
1
B12
B34
53
B76
103
N105
N109
B111
N121
B123
N127
126
B132
145
195
224
B238
244
B257
N261
N268 to N263
B269 N269 B2.269
B279 B282 B283
B286 B287 B289 N292
B296
TS-317
B318
B339
B355
TS-367
Hylogger scanner:
SWIR domain Mineralogical group
INVALID
SULPHATE
CARBONATE
CHLORITE
SMECTITE
WHITE-MICA
KAOLIN
TIR domain Mineralogical group
SULPHATE
CARBONATE
CHLORITE
SMECTITE
WHITE-MICA
KAOLIN
PLAGIOCLASE
SILICA
Composite log:
FAm1 Polygenic Breccia
FAm2 Thick-bedded sst
FAm3 M.-bedded sst
FAm4/5 Thin-bedded sst
FAm6 Mudrock
FAc1 Bioclastic GST
FAc2/3 Bioclastic PST
FAc4 Micritic MST
No exposure
Grain size
Cl= clay
vF= very fine
M= medium
vC= very coarse
Pbl= pebble
Bioturbations
Figure caption:
ex: Fig.8
Samples:
Mineralogical point counting
Petrography
Biostratigraphy

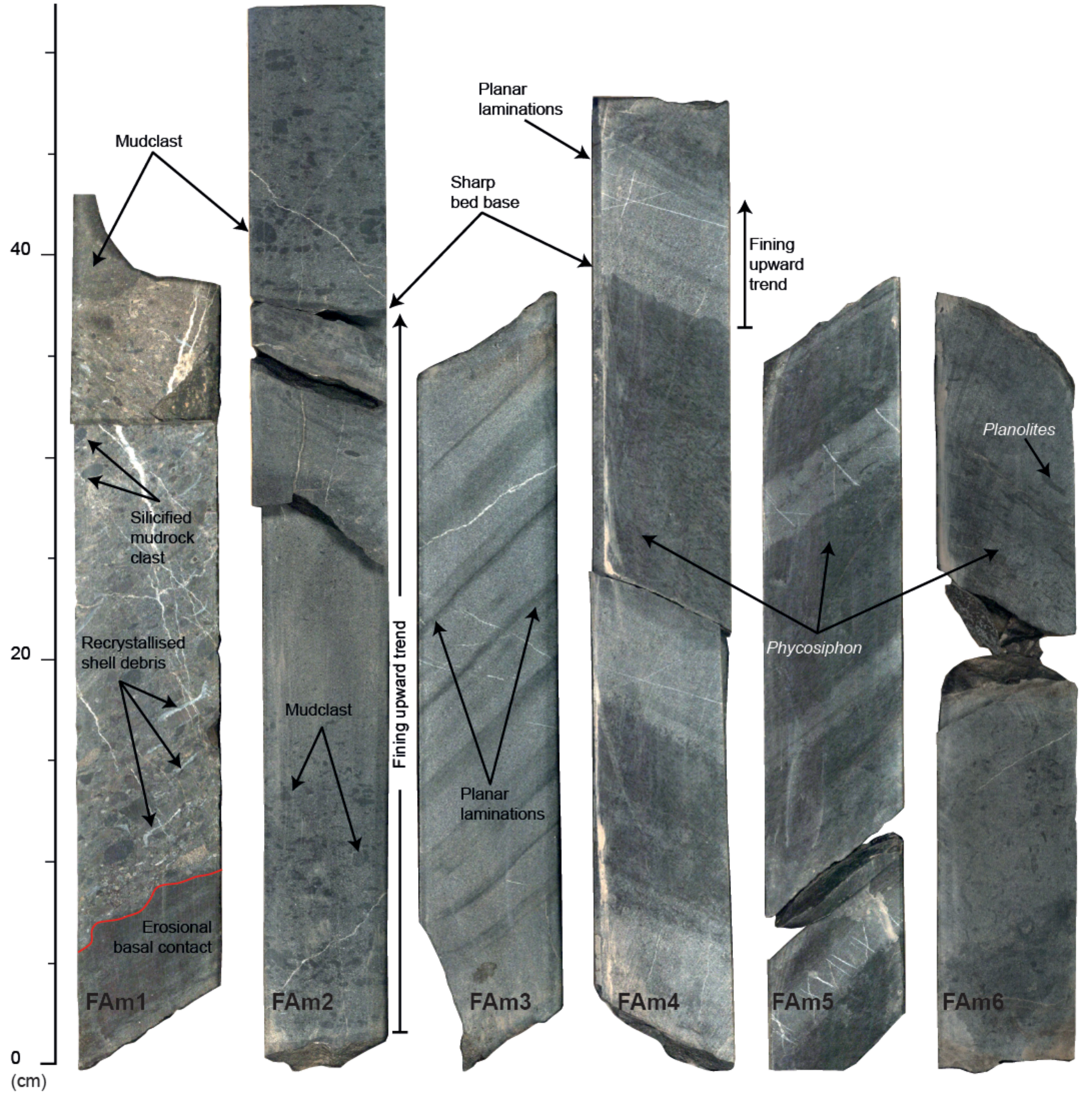

40
20
0
(cm)
Mudclast
Silicified
mudrock
clast
Recrystallised
shell debris
Erosional
basal contact
FAm1
Sharp
bed base
Fining upward trend
Mudclast
FAm2
Planar
laminations
FAm3
Planar
laminations
Fining
upward
trend
FAm4
Phycosiphon
FAm5
Planolites
FAm6

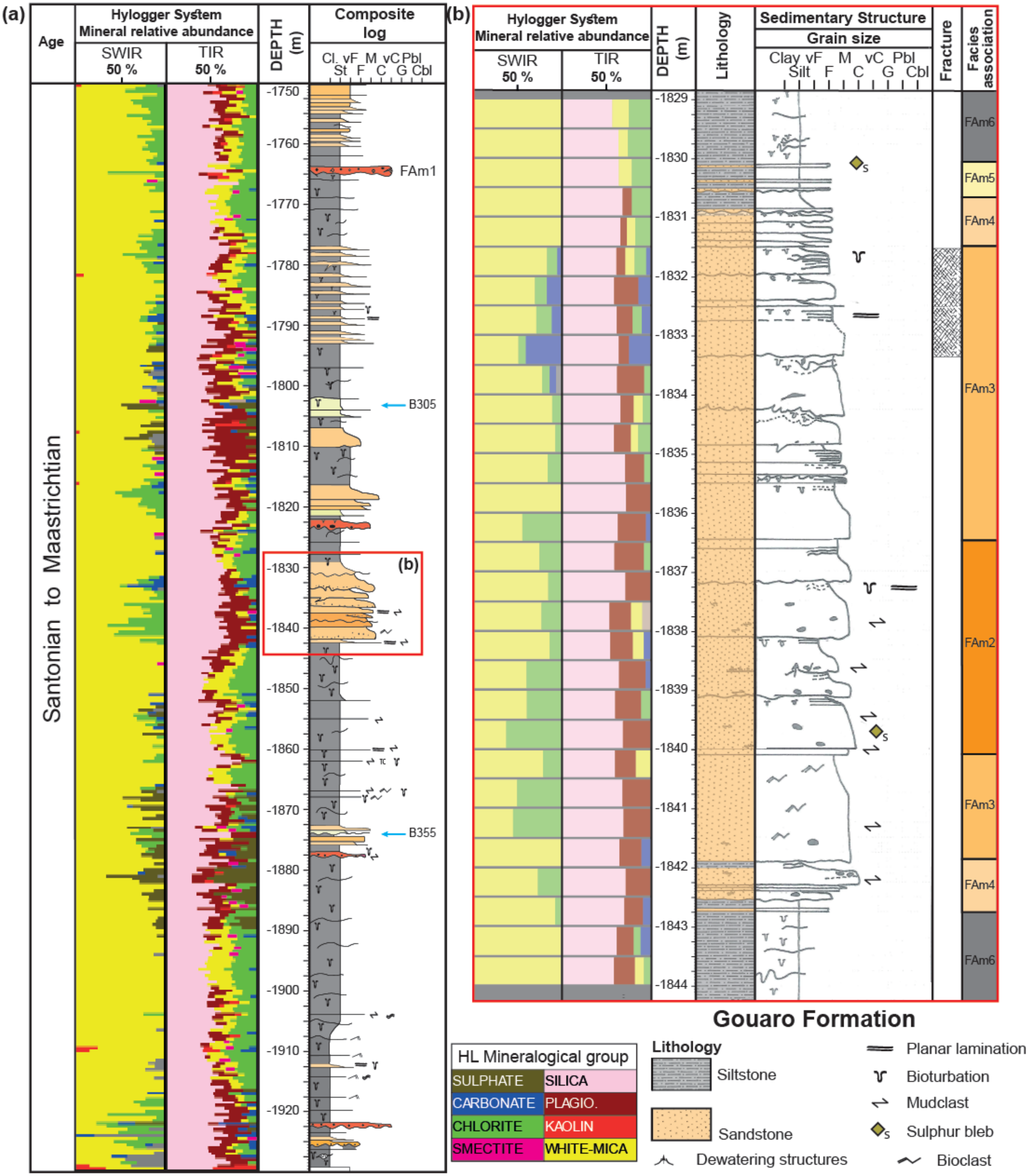

(a)
Age
Hylogger System
Mineral relative abundance
SWIR
50 %
TIR
50 %
DEPTH (m)
Composite log
Cl. vF M vC Pbl
St F C G Cbl
Santonian to Maastrichtian
FAm1
B305
B355
(b)
Hylogger System
Mineral relative abundance
SWIR
50 %
TIR
50 %
DEPTH (m)
Lithology
Sedimentary Structure
Grain size
Clay vF M vC Pbl
Silt F C G Cbl
Fracture
Facies association
FAm6
FAm5
FAm4
FAm3
FAm2
FAm3
FAm4
FAm6
Gouaro Formation
HL Mineralogical group
SULPHATE
SILICA
CARBONATE
PLAGIO.
CHLORITE
KAOLIN
SMECTITE
WHITE-MICA
Lithology
Siltstone
Sandstone
Dewatering structures
Planar lamination
Bioturbation
Mudclast
Sulphur bleb
Bioclast

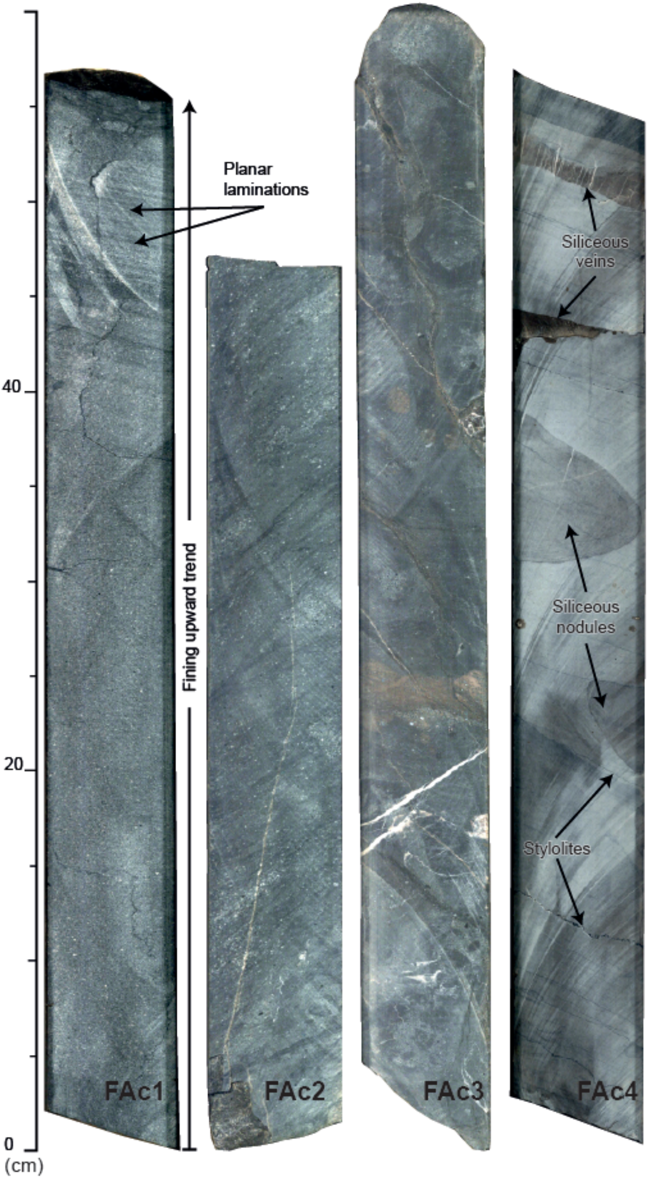

Planar laminations
Fining upward trend
Siliceous veins
Siliceous nodules
Stylolites
FAc1
FAc2
FAc3
FAc4
40
20
0
(cm)

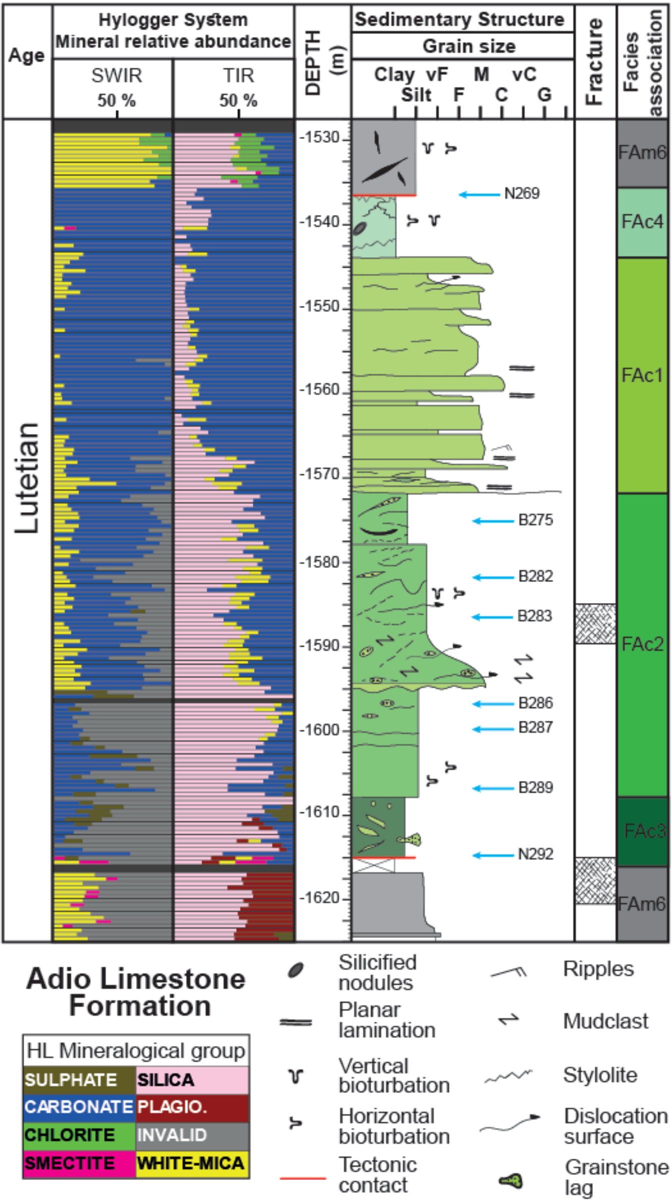

Age
Hylogger System
Mineral relative abundance
SWIR
50 %
TIR
50 %
DEPTH (m)
Sedimentary Structure
Grain size
Clay
Silt
vF
F
M
C
vC
G
Fracture
Facies association
Lutetian
-1530
-1540
-1550
-1560
-1570
-1580
-1590
-1600
-1610
-1620
N269
B275
B282
B283
B286
B287
B289
N292
FAm6
FAc4
FAc1
FAc2
FAc3
FAm6
Adio Limestone Formation
HL Mineralogical group
SULPHATE
SILICA
CARBONATE
PLAGIO.
CHLORITE
INVALID
SMECTITE
WHITE-MICA
Silicified nodules
Planar lamination
Vertical bioturbation
Horizontal bioturbation
Tectonic contact
Ripples
Mudclast
Stylolite
Dislocation surface
Grainstone lag

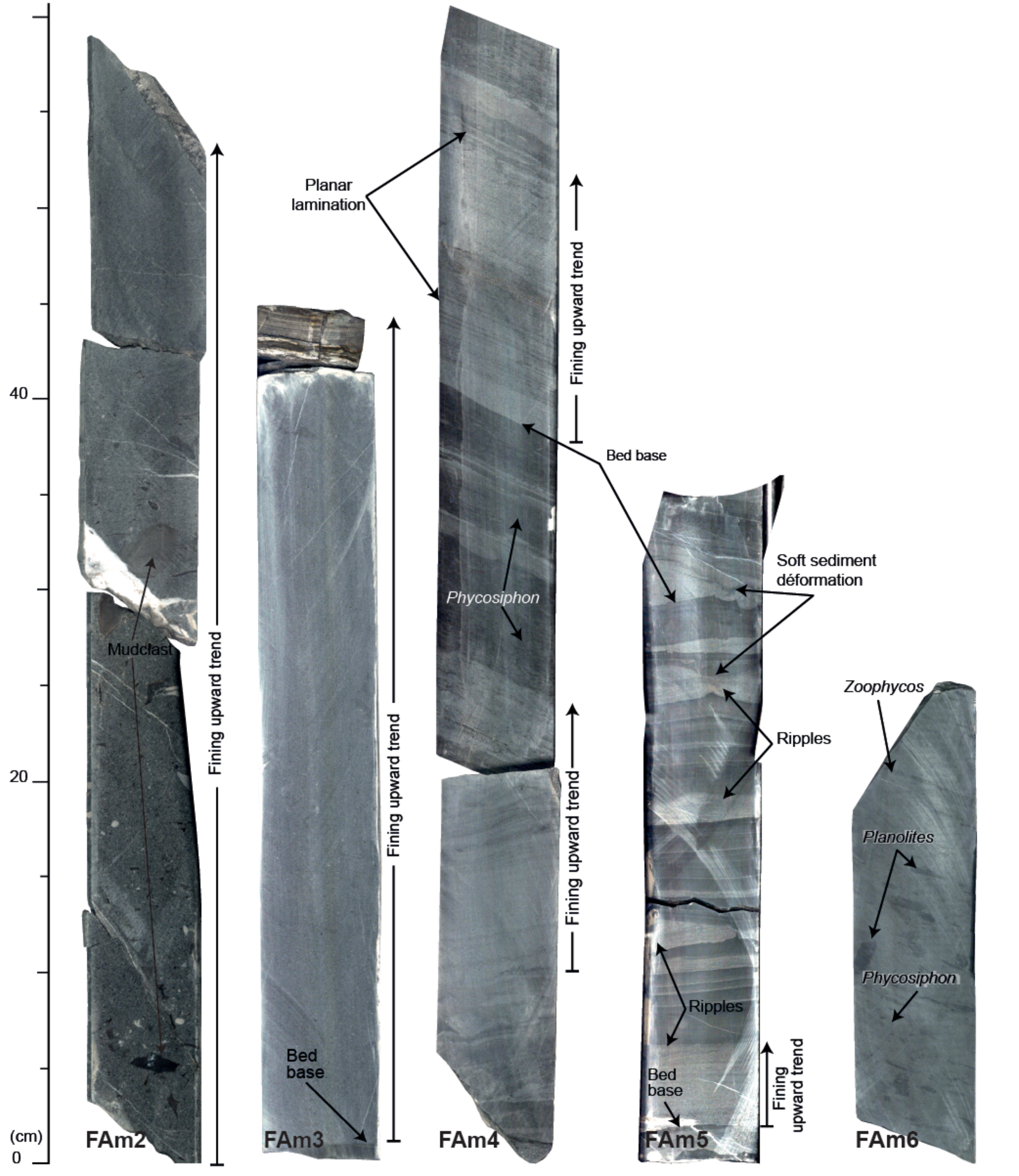

40
20
(cm)
0
Mudclast
Fining upward trend
FAm2
Bed
base
FAm3
Planar
lamination
Phycosiphon
Bed base
FAm4
Soft sediment
déformation
Ripples
Ripples
Bed
base
FAm5
Zoophycos
Planolites
Phycosiphon
FAm6

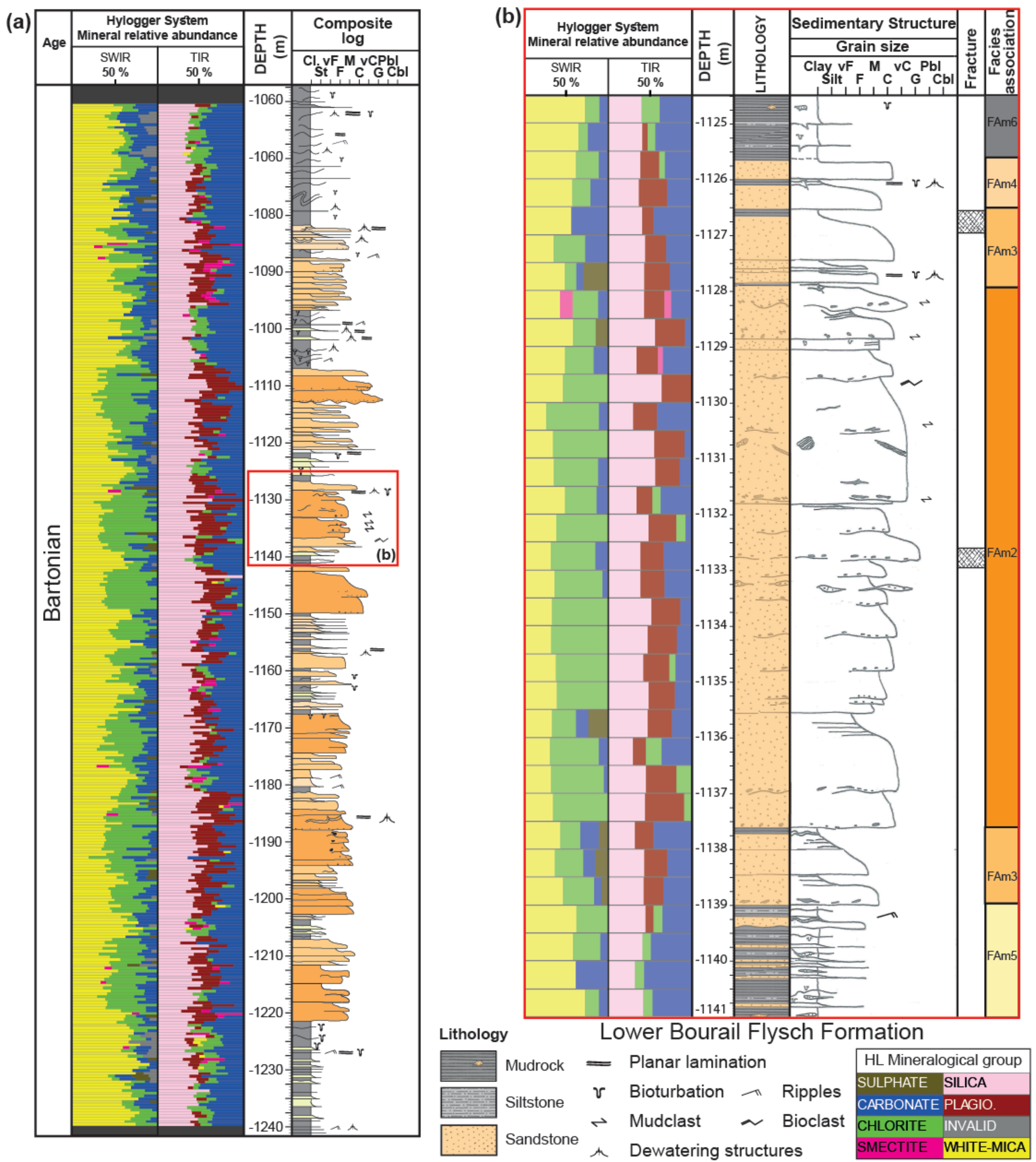

(a)
Age
Hylogger System
Mineral relative abundance
SWIR
50 %
TIR
50 %
DEPTH (m)
Composite log
Cl. vF M vCPbl
St F C G Cbl
Bartonian
(b)
Hylogger System
Mineral relative abundance
SWIR
50 %
TIR
50 %
DEPTH (m)
LITHOLOGY
Sedimentary Structure
Grain size
Clay vF M vC Pbl
Silt F C G Cbl
Fracture
Facies association
FAm6
FAm4
FAm3
FAm2
FAm3
FAm5
Lower Bourail Flysch Formation
Lithology
Mudrock
Siltstone
Sandstone
Planar lamination
Bioturbation
Mudclast
Dewatering structures
Ripples
Bioclast
HL Mineralogical group
SULPHATE
SILICA
CARBONATE
PLAGIO.
CHLORITE
INVALID
SMECTITE
WHITE-MICA

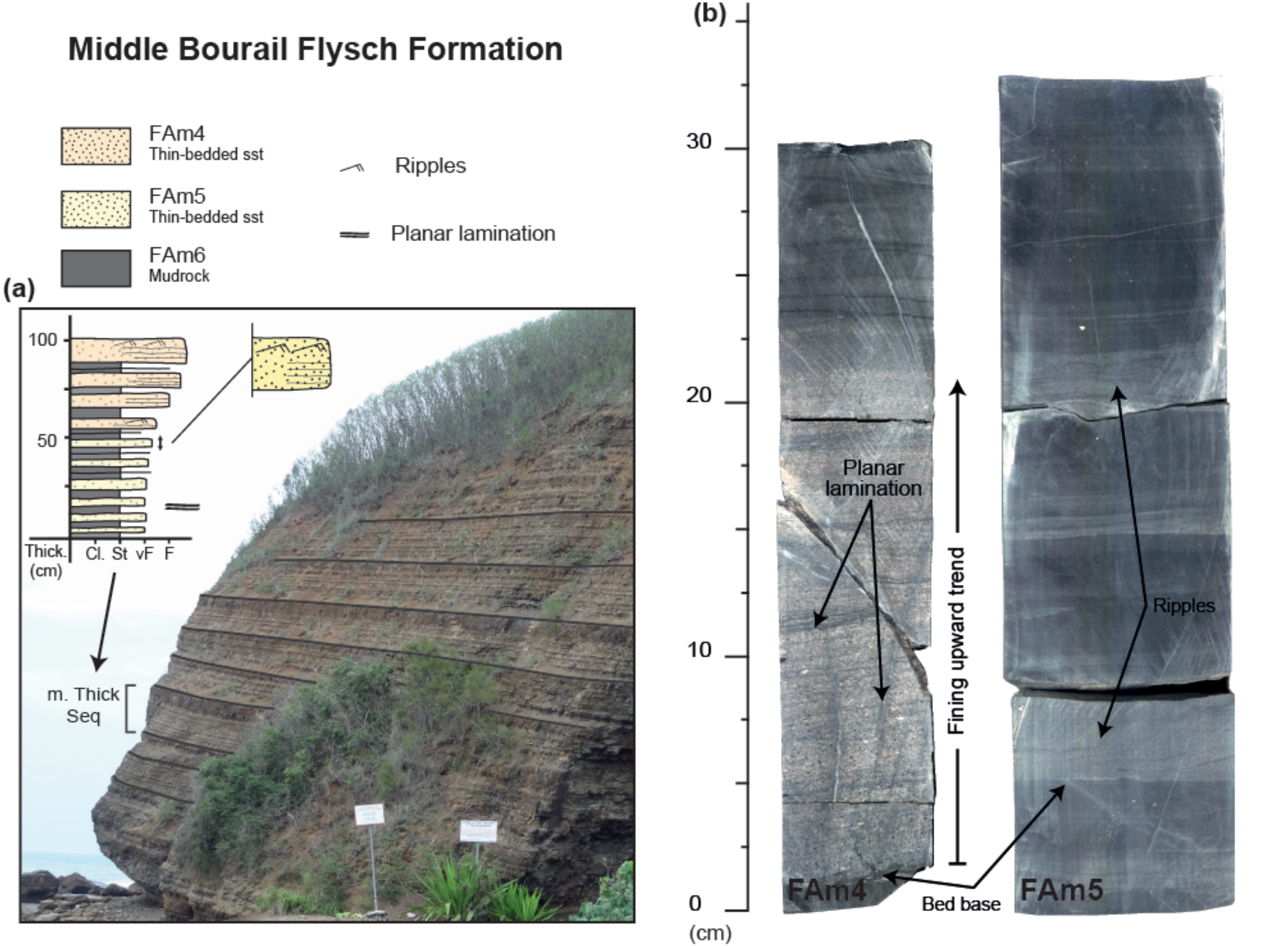

Middle Bourail Flysch Formation
FAm4
Thin-bedded sst
FAm5
Thin-bedded sst
FAm6
Mudrock
Ripples
Planar lamination
(a)
100
50
Thick.
(cm)
Cl.
St
vF
F
m. Thick
Seq
(b)
30
20
10
0
(cm)
Planar
lamination
Fining upward trend
Ripples
FAm4
Bed base
FAm5

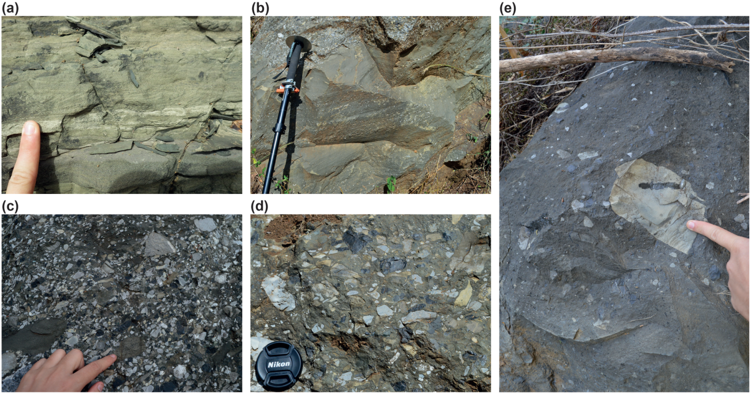
(a)
(b)
(c)
(d)
(e)
Nikon

(a)

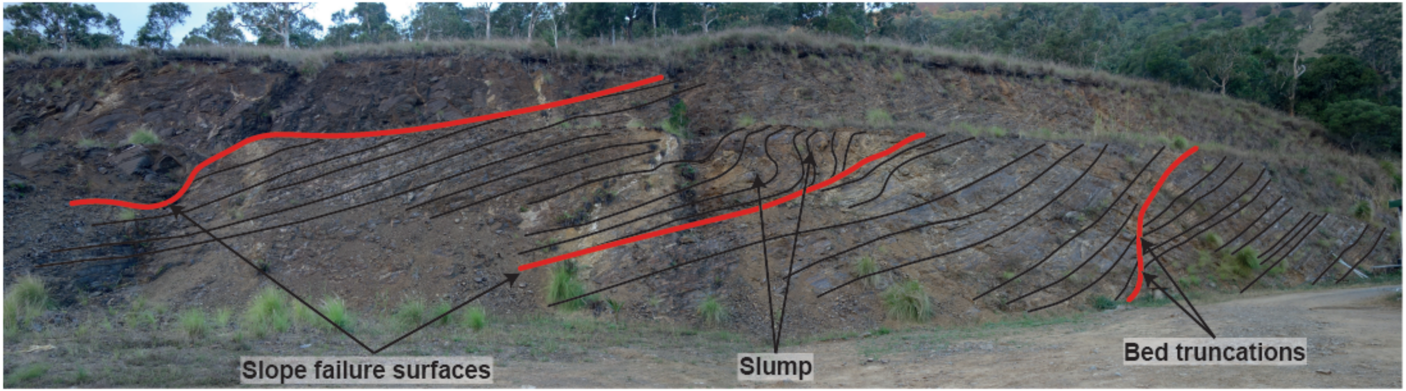
Slope failure surfaces
Slump
Bed truncations

(b)

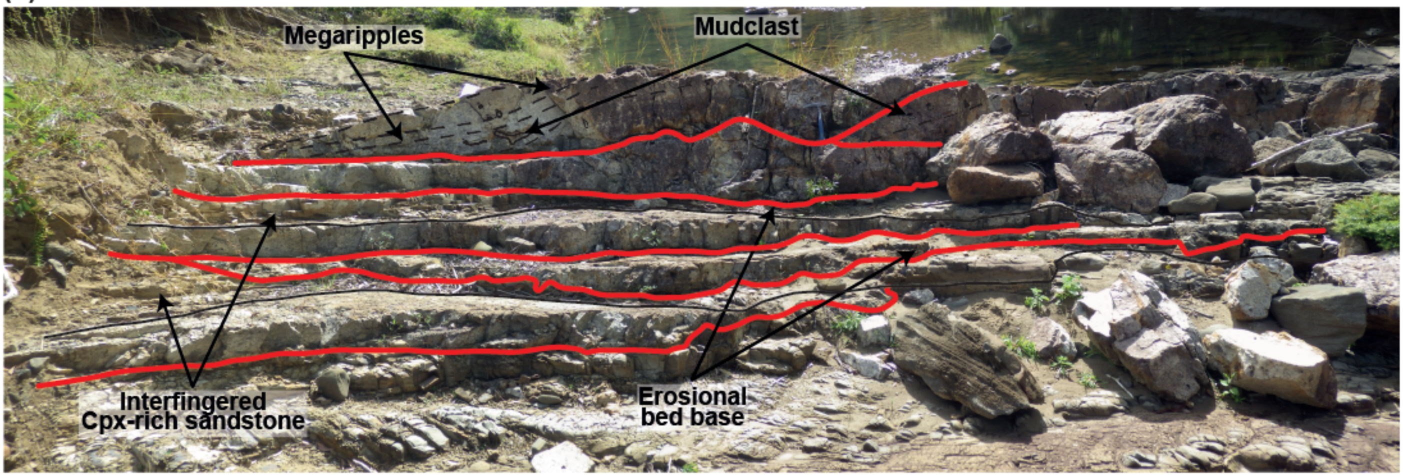
Megaripples
Mudclast
Interfingered
Cpx-rich sandstone
Erosional
bed base

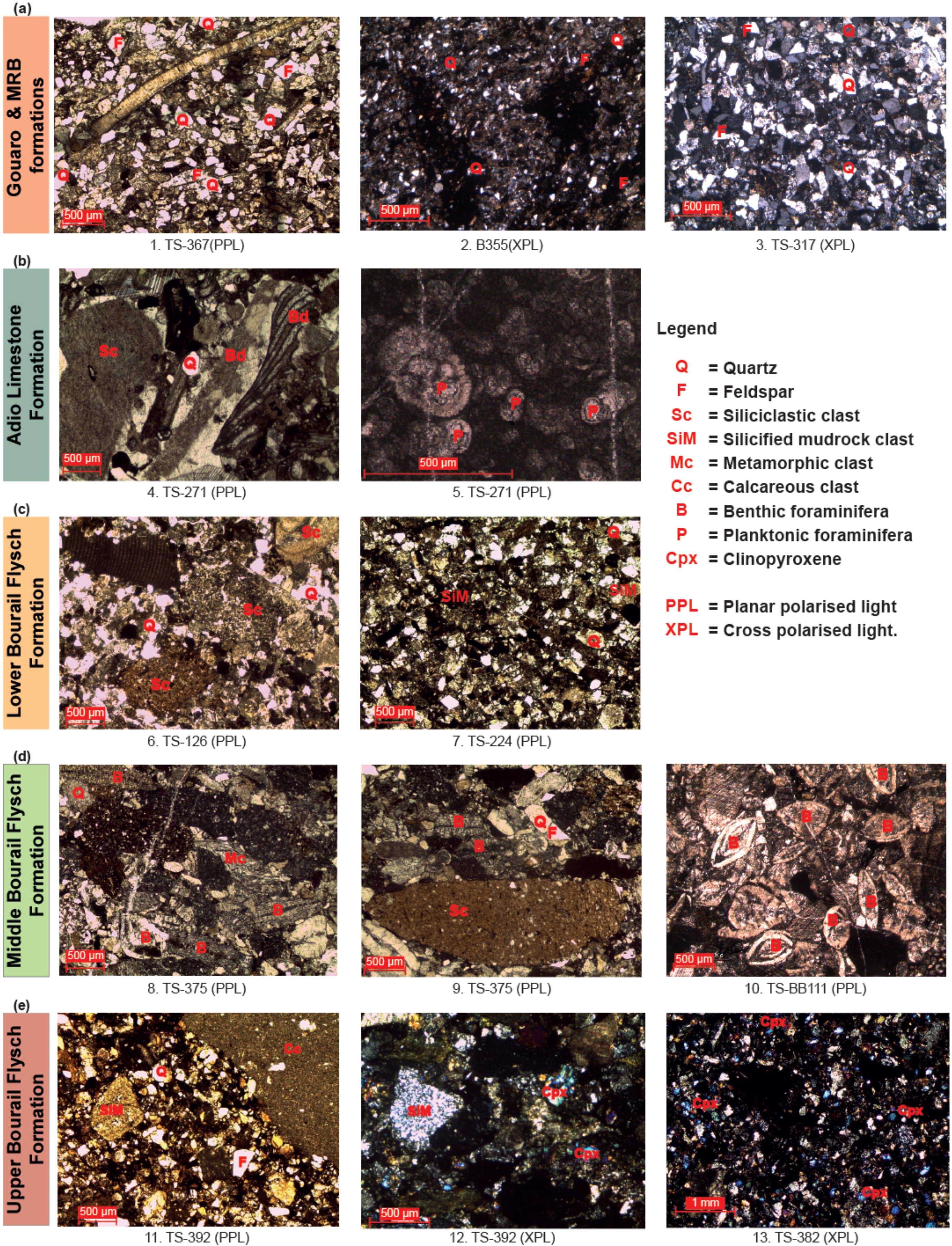
(a)
Gouaro & MRB formations
1. TS-367(PPL)
2. B355(XPL)
3. TS-317 (XPL)
(b)
Adio Limestone Formation
4. TS-271 (PPL)
5. TS-271 (PPL)
Legend
Q = Quartz
F = Feldspar
Sc = Siliciclastic clast
SiM = Silicified mudrock clast
Mc = Metamorphic clast
Cc = Calcareous clast
B = Benthic foraminifera
P = Planktonic foraminifera
Cpx = Clinopyroxene
PPL = Planar polarised light
XPL = Cross polarised light.
(c)
Lower Bourail Flysch Formation
6. TS-126 (PPL)
7. TS-224 (PPL)
(d)
Middle Bourail Flysch Formation
8. TS-375 (PPL)
9. TS-375 (PPL)
10. TS-BB111 (PPL)
(e)
Upper Bourail Flysch Formation
11. TS-392 (PPL)
12. TS-392 (XPL)
13. TS-382 (XPL)
500 µm
1 mm

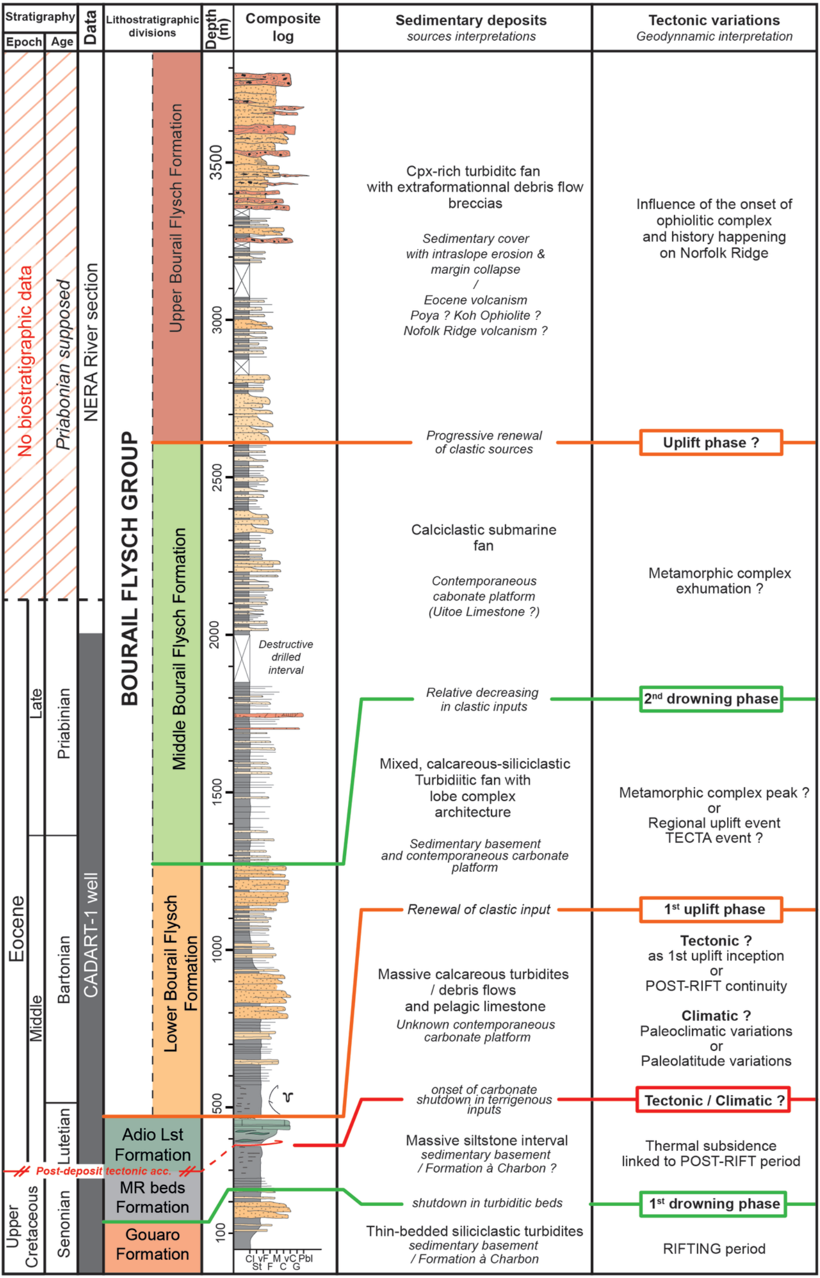

Stratigraphy
Epoch
Age
Data
Lithostratigraphic divisions
Depth (m)
Composite log
Sedimentary deposits
sources interpretations
Tectonic variations
Geodynnamic interpretation
No biostratigraphic data
Priabonian supposed
NERA River section
CADART-1 well
Eocene
Late
Middle
Priabinian
Bartonian
Lutetian
Upper Cretaceous
Senonian
BOURAIL FLYSCH GROUP
Upper Bourail Flysch Formation
Middle Bourail Flysch Formation
Lower Bourail Flysch Formation
Adio Lst Formation
MR beds Formation
Gouaro Formation
Post-deposit tectonic acc.
3500
3000
2500
2000
1500
1000
500
100
Destructive drilled interval
Cl vF M vC Pbl
St F C G
Cpx-rich turbiditc fan with extraformationnal debris flow breccias
Sedimentary cover with intraslope erosion & margin collapse / Eocene volcanism Poya ? Koh Ophiolite ? Nofolk Ridge volcanism ?
Influence of the onset of ophiolitic complex and history happening on Norfolk Ridge
Progressive renewal of clastic sources
Uplift phase ?
Calciclastic submarine fan
Contemporaneous cabonate platform (Uitoe Limestone ?)
Metamorphic complex exhumation ?
Relative decreasing in clastic inputs
2nd drowning phase
Mixed, calcareous-siliciclastic Turbidiitic fan with lobe complex architecture
Sedimentary basement and contemporaneous carbonate platform
Metamorphic complex peak ? or Regional uplift event TECTA event ?
Renewal of clastic input
1st uplift phase
Tectonic ? as 1st uplift inception or POST-RIFT continuity
Climatic ? Paleoclimatic variations or Paleolatitude variations
Massive calcareous turbidites / debris flows and pelagic limestone
Unknown contemporaneous carbonate platform
onset of carbonate shutdown in terrigenous inputs
Tectonic / Climatic ?
Massive siltstone interval
sedimentary basement / Formation à Charbon ?
Thermal subsidence linked to POST-RIFT period
shutdown in turbiditic beds
1st drowning phase
Thin-bedded siliciclastic turbidites
sedimentary basement / Formation à Charbon
RIFTING period

	Lithofacies	Code	Description	Flow Types
Calcareous facies association	Thick bedded bioclastic grainstone	FAc1	Light-grey, thick bedded, sharp to erosional based, homogeneous to normally graded, medium to coarse-grained with some sharp grain size increase; massive to plane-laminated bioclastic limestone with a grainstone texture and preserved bed top in some case	Hyper to concentrated flow / By-passing flow
	Massive to normally graded bioclastic packstone	FAc2	Light-grey, heterogeneous, faint or deformed plane-laminated, strongly deformed by soft sediment deformation bioclastic limestone with a packstone texture. Plane laminations are marked by fine to medium grained bioclastic lamina.	?
	Bioclastic lime-siliciclastic wackstone	FAc3	Dark grey homogeneous, bioturbated (Planolites) and massive calcareous siltstone with a wackstone texture and several bioclastic interval deformed by soft sediment deformation	?
	Mudstone with planktonic foraminifera	FAc4	Massive and homogeneous micritic limestone with a mudstone texture with planktonic foraminifers. Several centimeter thick silicifieous nodules and compaction structures are present (stylolite).	Pelagic fall-out
Calcareous / siliciclastic / clinopyroxene mixed sources facies association	Sandy matrix polygenic breccia	FAm1	Massive to normally graded, clast supported, sandy matrix breccia. Clast are poorly sorted, angular, and polygenic. Clast size varies from medium pebbles to cobbles. In some case, traction carpet are present as layer in disorganized breccia. Several decimeter to several meter thick bed observe erosional basal contact as amalgamated basal surface or by-pass surfaces.	Grain flow
	Thick-bedded granular to coarse-grained sandstone	FAm2	Normally graded or massive very coarse to coarse grained sandstone. Facies is organized as several decimeter to meter thick bed with basal erosional by-passing surfaces and centimeter thick mudclast lag. Planar laminations are observed at top of beds and dewatering structures as dishes are present.	Hyperconcentrated flow
	Thick-bedded coarse to medium-grained sandstone	FAm3	Normally graded coarse to medium grained sandstone. Several decimeter to meter thick beds has sharp base contact or erosional base surface as amalgamation. Grain size is fining upward from medium / coarse to fine. Planar lamination overlie by ripples forms top of bed and bed caps are preserved.	Concentrated flow
	Interbedded sandstone and siltstone (sandy heterolithics)	FAm4	Normally graded several centimeter to decimeter thick medium grained sandstone, interbedded with several centimeter thick homogeneous and bioturbated siltstone. Sandstone beds correspond to Bouma classical turbidites sequence with top-missing sequence (td, te). Tabc Bouma terms are present. Grain size is fining upward to muddy bed caps with bioturbations. Basal contact are sharp and flute or groove cast are also preserved.	Turbidity current
	Interbedded sandstone and siltstone (muddy heterolithic)	FAm5	Normally graded centimeter thick fine grained sandstone interbedded with several centimeter to decimeter thick homogeneous and bioturbated siltstone (Fe6). Sandstone beds correspond to Bouma classical turbidites sequence with base-missing sequence (ta). Tbcde terms are preserved. Grain size is fining upward to muddy bed caps with bioturbations. Basal contacts are sharp.	Turbidity current
	Bioturbated massive siltstone / mudrock	FAm6	Massive and homogeneous siltstone highly bioturbated. Nereites, Zoophycos and Phycosyphon represent majority of bioturbations	Hemipelagic fall-out

	Lithofacies	Code	Description	Flow Types	Simplfied lithofacies log
Calcareous facies association	Thick bedded bioclastic grainstone	FAc1	Light-grey, thick bedded, sharp to erosional based, homogeneous to normally graded, medium to coarse-grained with some sharp grain size increase; massive to plane-laminated bioclastic limestone with a grainstone texture and preserved bed top in some case	Hyper to concentrated flow / By-passing flow	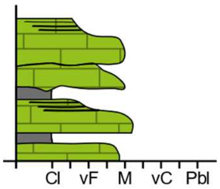
	Massive to normally graded bioclastic packstone	FAc2	Light-grey, heterogeneous, faint or deformed plane-laminated, strongly deformed by soft sediment deformation bioclastic limestone with a packstone texture. Plane laminations are marked by fine to medium grained bioclastic lamina.	?	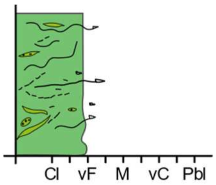
	Bioclastic lime-siliciclastic wackstone	FAc3	Dark grey homogeneous, bioturbated (Planolites) and massive calcareous siltstone with a wackstone texture and several bioclastic interval deformed by soft sediment deformation	?	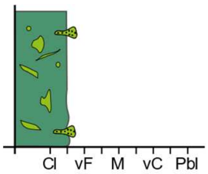
	Mudstone with planktonic foraminifera	FAc4	Massive and homogeneous micritic limestone with a mudstone texture with planktonic foraminifers. Several centimeter thick silicifieous nodules and compaction structures are present (stylolite).	Pelagic fall-out	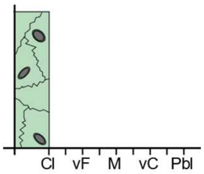
Calcareous / siliciclastic / clinopyroxene mixed sources facies association	Sandy matrix polygenic breccia	FAm1	Massive to normally graded, clast supported, sandy matrix breccia. Clast are poorly sorted, angular, and polygenic. Clast size varies from medium pebbles to cobbles. In some case, traction carpet are present as layer in disorganized breccia. Several decimeter to several meter thick bed observe erosional basal contact as amalgamated basal surface or by-pass surfaces.	Grain flow	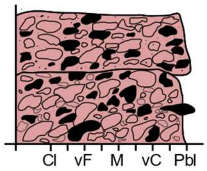
	Thick-bedded granular to coarse-grained sandstone	FAm2	Normally graded or massive very coarse to coarse grained sandstone. Facies is organized as several decimeter to meter thick bed with basal erosional by-passing surfaces and centimeter thick mudclast lag. Planar laminations are observed at top of beds and dewatering structures as dishes are present.	Hyperconcentrated flow	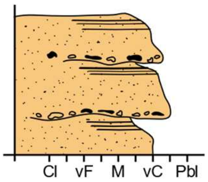
	Thick-bedded coarse to medium-grained sandstone	FAm3	Normally graded coarse to medium grained sandstone. Several decimeter to meter thick beds has sharp base contact or erosional base surface as amalgamation. Grain size is fining upward from medium / coarse to fine. Planar lamination overlie by ripples forms top of bed and bed caps are preserved.	Concentrated flow	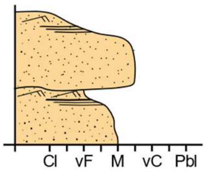
	Interbedded sandstone and siltstone (sandy heterolithics)	FAm4	Normally graded several centimeter to decimeter thick medium grained sandstone, interbedded with several centimeter thick homogeneous and bioturbated siltstone. Sandstone beds correspond to Bouma classical turbidites sequence with top-missing sequence (td, te). Tabc Bouma terms are present. Grain size is fining upward to muddy bed caps with bioturbations. Basal contact are sharp and flute or groove cast are also preserved.	Turbidity current	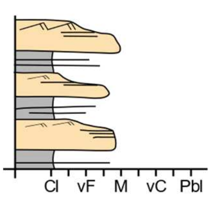
	Interbedded sandstone and siltstone (muddy heterolithic)	FAm5	Normally graded centimeter thick fine grained sandstone interbedded with several centimeter to decimeter thick homogeneous and bioturbated siltstone (Fe6). Sandstone beds correspond to Bouma classical turbidites sequence with base-missing sequence (ta). Tbcde terms are preserved. Grain size is fining upward to muddy bed caps with bioturbations. Basal contacts are sharp.	Turbidity current	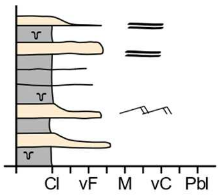
	Bioturbated massive siltstone / mudrock	FAm6	Massive and homogeneous siltstone highly bioturbated. Nereites, Zoophycos and Phycosyphon represent majority of bioturbations	Hemipelagic fall-out